Progress in Biomass Electro-Valorization for Paired Electrosynthesis of Valuable Chemicals and Fuels

Amira Ben Abderrahmane, Sophie Tingry, David Cornu, Yaovi Holade

Progress in Biomass Electro-Valorization for Paired Electrosynthesis of Valuable Chemicals and Fuels

*Amira Ben Abderrahmane, Sophie Tingry, David Cornu and Yaovi Holade**

A. Ben Abderrahmane, S. Tingry, D. Cornu, Y. Holade
Institut Européen des Membranes, IEM, UMR 5635, Univ Montpellier, ENSCM, CNRS, 34090 Montpellier, France
E-mail: yaovi.holade@enscm.fr (Y.H.)

A. Ben Abderrahmane, S. Tingry, D. Cornu, Y. Holade
French Research Network on Hydrogen (FRH2), Research Federation No. 2044 CNRS, https://frh2.cnrs.fr/
44322 Nantes Cedex 3, France

Keywords: anion exchange membrane; biomass conversion; electrocatalytic oxidation; hydrogen production; paired electrosynthesis

Abstract.
Environmental and energy concerns surrounding the use of fossil fuels are driving an increasingly rapid transition to sustainable and eco-responsible processes. Electrochemical processes could provide the necessary sustainability and economic roadmap for storing intermittent and renewable electricity by synthesizing, in cogeneration electrolyzers, energy carriers and/or synthetic chemicals (H_2, NH_3, etc.) via flagship reduction reactions (HER, CO2RR, NRR, etc.). To balance the electrochemical process, these cathodic processes have long been coupled to the oxygen evolution reaction (OER), which ends up consuming almost 90% of the input energy. Recent years have witnessed an overwhelming development of anode scenarios based on biomass substrates, because OER cannot be driven below a certain potential threshold, while organics are thermodynamically more favorable. Therefore, paired electrolysis, which refers to cases where electrochemical oxidation and reduction are desired, embraces the electrocatalysis community for the electrolytic production of H_2, NH_3, etc. (cathode side), in parallel, value-added chemicals (anode side), all with a modest input of electricity. The trade-off is selectivity at a relevant current density. This review discusses the progress, challenges,

and potential of biomass-fueled paired electrosynthesis of valuable chemicals and fuels. Fundamental principles, main biomass solubilization methods, and different scenarios for paired electrosynthesis are presented.

1. Introduction

The Sixth Assessment Report of the Intergovernmental Panel on Climate Change (IPCC) has highlighted the observed impacts of human-induced climate change on all forms of life on Earth, from ecosystems to human civilization.[1] Rising carbon dioxide (CO_2) emissions represent the major source of global warming. The emission of these greenhouse gases traps heat in the atmosphere. To limit the excess of greenhouse gases, forests and green spaces should be increased so that nature can absorb some of the CO_2 emissions. However, deforestation has increased in recent years, resulting in the disappearance of large areas of forest to make way for crops or pastures, which contain less organic matter and therefore can absorb less CO_2.[1] To reduce the risks of climate change, it is essential to adapt our existing systems and make an energy transition to avoid burning fossil fuels to produce energy for our activities. In this context, dihydrogen (H_2) is seen as a promising energy carrier. In particular, because of its ability to store energy produced by intermittent sources (solar, wind, hydro), allowing electricity production to be regulated. It can also be used as a fuel in fuel cell vehicles, which do not emit greenhouse gases and are therefore an alternative to fossil fuel vehicles.[2,3]

One of the challenges to be overcome if H_2 is to become a widespread energy solution is to develop more cost-effective and sustainable production methods. Today, for economic reasons, 95% of H_2 is produced from fossil fuels by steam reforming, which generates substantial quantities of CO_2 (over 830 million tons per year).[4,5] One of the alternatives to this highly polluting production method is water electrolysis. This method consists of splitting water (H_2O) into dioxygen (O_2, anodic side) and H_2 (cathodic side) using an electric current. It allows sustainable H_2 production, but has the disadvantage of being energy-intensive because of the high potential of the O_2 evolution reaction (OER). In fact, owing to kinetic limitations, an excess cell voltage is required alongside the theoretical decomposition voltage of 1.23 V when considering the standard conditions. It should be noted that, thermodynamically, the conversion of the liquid reactant (H_2O) into gaseous products (H_2 and O_2) requires additional energy resulting from the increase in entropy.[6-8] Therefore, under standard conditions, water electrolysis (splitting) never starts at $U°$ = 1.23 V, contrary to certain misconceptions resulting exclusively from the respective standard potentials of the involved redox pairs H^+/H_2 ($E°$ = 0 V vs RHE (reversible hydrogen electrode[9])) and O_2/H_2O ($E°$ = 1.23 V vs RHE). Thus, the

thermo-neutral voltage, taking into account the entropy, is $U°$ = 1.4-1.5 V for $2H_2O \rightarrow 2H_2 + O_2$, which can be deduced from the elementary calculation using enthalpy variation ($U° = -\Delta_r H°/nF$, n being the electrons transferred per H_2O molecule reacted and F being the Faraday constant) instead of using free enthalpy variation ($U° = -\Delta_r G°/nF$). To minimize electricity consumption, biomass substrates can be used as feedstock in a co-production electrolyzer that produces valuable chemicals (anode) and fuels such as H_2 or NH_3 (cathode). In fact, cellulose is a primary constituent of plant cell walls,[10] and together with hemicelluloses and lignin, these substrates can feed electrolyzers for cogeneration of renewable fuels and chemicals. Biomass-fed electrolyzers are likely to require a lower cell voltage (U) than conventional electrolyzers due to the low oxidation potential of organic substrates compared to OER. This results in lower energy consumption according to Equation (1), which is also shown in **Figure 1**.[11]

$$U_{cell} = E_{(+)} - E_{(-)} = E_{anode} - E_{cathode} \quad (1)$$

To achieve a double gain in terms of reaction products and electricity consumption, it is necessary to find optimal conditions for the solubilization of cellulosic biomass. In addition, efficient electrode materials with high electrocatalytic performances (selectivity, activity, durability) as well as suitable membranes for the final electrolysis cell system need to be developed. However, given the diversity of biomass substrates, the development of nanostructured electrocatalysts to reduce the cost and evaluate new functionality remains a challenge for the electrocatalytic upgrading of biomass, as we currently do not know the driving forces for efficient electron transfer and product/reagent transport to/from the electrocatalyst surface.[12-15] For example, cellulose (molecular weight of 10^3-10^5 g mol^{-1}[16]), which represents 30-50% of biomass and is a polymer of glucose (DP1) or cellobiose (DP2), can be selectively oxidized to produce gluconate, glucuronate or glucarate, which are of great interest as food additives, pharmaceutical raw materials, construction and paper industries.[12,17,18] In particular, the attractiveness and promise of biomass electroconversion (or electroreforming) of raw cellulose has been greatly appreciated in the last decade. However, inter/intra-molecular hydrogen bonding hinders the solubility of polymeric cellulose, 1 to 60 g per L, which is relatively small given the high molecular weight of 10^3-10^5 g mol^{-1}.[16,19,20] Therefore, it is difficult to conceive high performance electrolyzers in forging paired electrolysis that can achieve selective oxidation at high current density (>0.2 A cm^{-2}, which would correspond to a co-production of 0.1 L(H_2)/h per cm^2 at the cathode) without any CO_2 problems. The main challenge lies in the limited fundamental understanding of the control of electrocatalytic

selectivity at high current density, which is necessary to achieve significant conversions and then H_2 or NH_3 productivities, because C-C bond cleavage leads to CO_2 or CO,[12,21-26] which nullifies the sustainability and economic aspects of the coupled electrosynthesis.

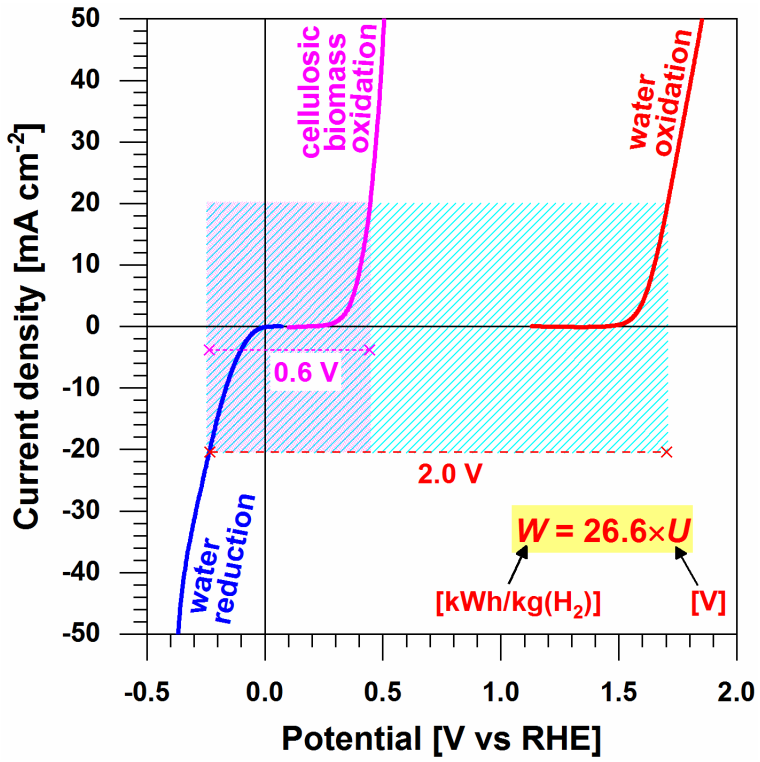

Figure 1. Polarization curves showing the sharp decrease in energy when water reduction into H_2 (HER, hydrogen evolution reaction) is coupled with the oxidation of cellulosic biomass molecules instead of water molecules (OER, oxygen evolution reaction). HER can be replaced by CO2RR or N2RR (CO_2 or N_2 reduction reaction) to produce commodity renewable chemicals at the cathode while the cellulosic biomass is selectively electrooxidized at the anode.

Paired electrosynthesis, i.e., the ability to simultaneously control the anode reaction and the cathode reaction during an electrochemical process to all lead to the formation of product(s), has been widely used in the synthetic organic electrochemistry community for decades.[27-33] This concept has been booming in the electrocatalysis community during the last decade due to the need to reduce energy consumption for better utilization of HER, CO2RR and NRR for the synthesis of green fuels (H_2, NH_3, CH_4, etc.).[12,21,34-51] Conceptually, paired electrosynthesis (coupled-electrolysis) offers the possibility of energy and time savings (200% current efficiency could be theoretically reached when the reaction product is the same at the cathode and at the anode. This review provides a comprehensive overview of the current research on the different scenarios of biomass-fueled paired electrosynthesis in the context of green synthesis of energy

carriers and/or synthetic chemicals through the flagship reductive reactions (HER, CO2RR, NRR, etc.). Specifically, we discuss the different scenarios for biomass-fueled paired electrolysis systems to identify the basic concepts, challenges, and key insights for moving forward. Although different types of biomass substrates can be used, the trade-off here is selectivity at high current densities (scalability and practicality levels of 0. 2-2 A cm^{-2}),[4] because in addition to the slow kinetics of organic electrooxidation, which is a proton-coupled electron transfer (PCET) process,[13-15,52-54] at higher potentials (>1.2-1.5 V vs. RHE) unwanted complete oxidation leading to CO_2-based species can occur, which seems to violate our original intent of reducing global warming through the application of electrochemical technologies.

2. Fundamentals of Electrolysis Cells

The implementation of electrochemical reactions requires the use of specific reactors that allow the conversion of electrical energy into chemical energy or vice versa. Depending on the direction of this conversion, electrolysis cells (**Figure 2a**) can be distinguished from fuel cells (**Figure 2b**). Regardless of the type of reactor, it consists of two electrically conductive materials forming the electrodes, separated by an ionic conductor (membrane, glass frit, etc.) that allows ion transfer and acts as an electron flow barrier. In both cells, two half-reactions – oxidation at the anode and reduction at the cathode – are paired together to form an overall reaction. The main difference between the two electrochemical cells is the polarity of the electrodes: for a fuel cell, the negative electrode is the anode and the positive electrode is the cathode, while the reverse is true for an electrolysis cell.[55,56]

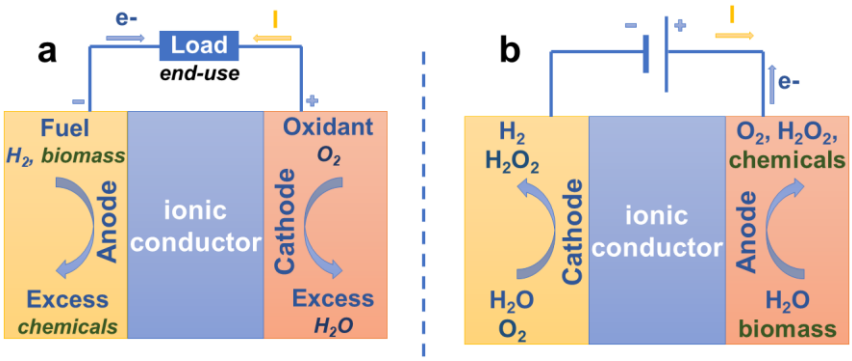

Figure 2. Schematic representation of a low-temperature (below 100-120 °C) electrochemical reactor operating as: a) a galvanic cell (fuel cell), and b) an electrolytic cell (electrolyzer).

A paired electrosynthesis system refers to an electrolysis cell (divided or undivided) in which both sides, oxidation and reduction reactions, are combined and contribute to the

production of either a single product or two separate products. Therefore, through paired electrosynthesis, both cathodic and anodic reactions can be optimized to increase energy efficiency, selectivity, and eliminate any generation of waste or unwanted by-products.[28,30] **Figure 3a** highlights the simplified mechanism of a chemical reaction A + B → P driven or not by the (electro)catalytic process. In conventional heterogeneous catalysis (solid/liquid, solid/gas or liquid/gas interface), a catalyst is used to lower the activation energy of a chemical reaction that is thermodynamically favorable under the conditions envisaged. In electrocatalysis, this activation energy barrier is further lowered by means of electronic transfer at the surface of the electrocatalyst, in order to transform an electroreactive species efficiently and in a controlled manner. This is achieved by controlling the reaction site, i.e. the catalyst/electrolyte interface. In heterogeneous phases, the surface of the electrocatalyst plays a decisive role. The total energy required to drive an electrolysis cell corresponds to the potential difference between the half reactions that take place at the anode and cathode. (**Figure 3b**). This makes the paired electrosynthesis an interesting choice in the sense that the energy used for both reactions produces a result, and no counter-reaction energy is wasted.[29,30]

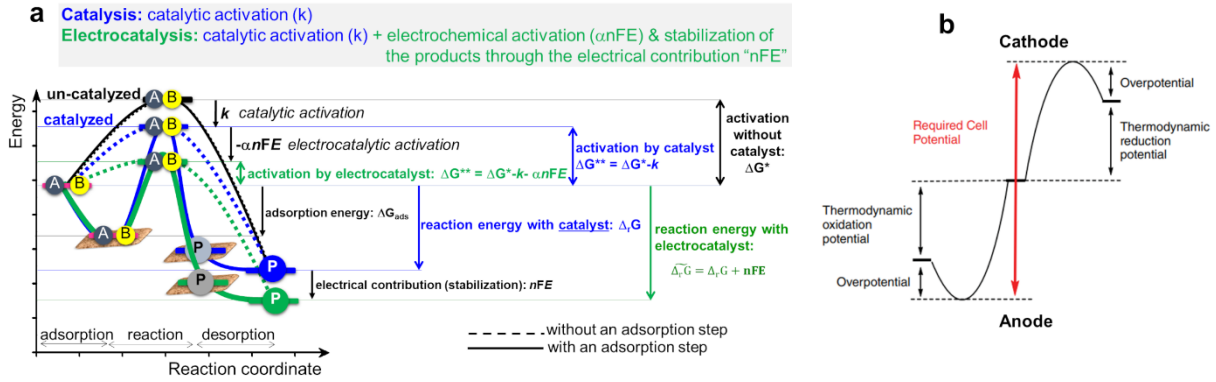

Figure 3. a) Effect of the electrocatalytic activation on the energy profiles of a (electro)catalytic reaction. b) Energy requirement for an electrolysis process; reprinted and adapted with permission from ref.[57], Copyright 2020, Wiley-VCH Verlag GmbH & Co.KGaA, Weinheim.

The four possible configurations of paired electrolysis systems are summarized in **Figure 4**.[28,50] The parallel paired electrolysis system refers to a split cell in which two different reactions are carried out simultaneously to obtain both cathodic and anodic products. It is important to emphasize that this type of system could require high manufacturing costs if the operating conditions such as solvent, pH, temperature, etc. are different between the two half-reactions. The concept of convergent paired electrolysis occurs in an undivided cell and

involves the production of a unique product resulting from the conversion of intermediates generated from the cathode and the anode. A divergent paired electrolysis involves the use of a common initial substrate at both electrodes, resulting in 2 different final products. In a linear paired electrolysis process, an identical product is formed from a common reactant by different electrochemical reactions using redox mediators[33] or different electrocatalysts[31] at the anode and cathode. For example, the electroconversion of dibutyl *N*-hydroxylamine to *N*-butylidenbutylamine N-oxide (nitrone) was performed using two redox mediators WO_5^{2-}/WO_4^{2-} (at the cathode) and Br_2/Br^- (anode), resulting in a linear paired electrosynthesis with a faradaic efficiency higher than 180%.[33]

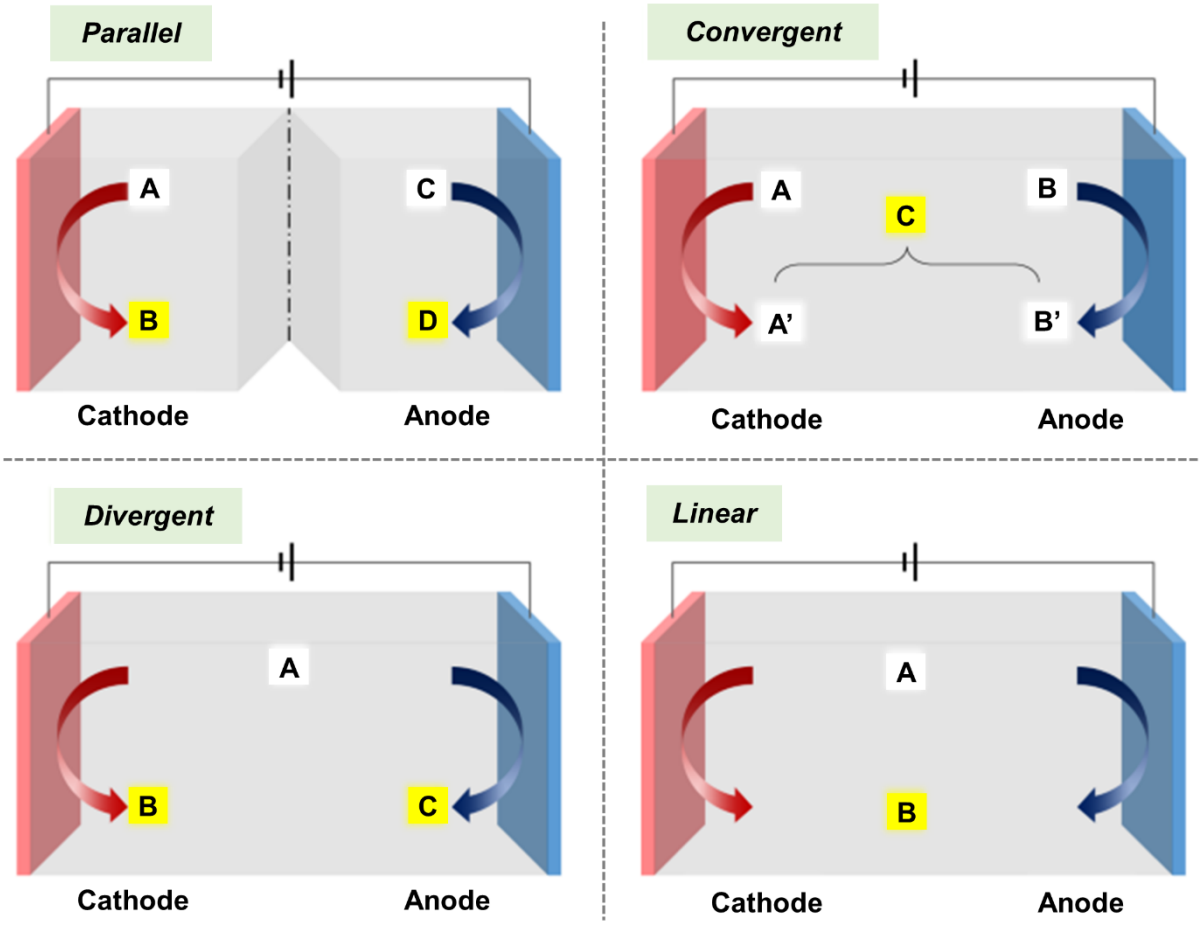

Figure 4. Schematic illustration of the four possible configurations of paired electrolysis systems: parallel (top, left), convergent (top, right), divergent (bottom, left), and linear (bottom, right). Reprinted and adapted with permission from ref.[50] under a CC BY 3.0 license, Copyright 2019, The Author(s), published by Springer Nature Limited.

For the paired electrolysis reactor assembly, **Figure 5a** represents the most basic configuration, the single compartment electrolysis cell. In this configuration, both reduction

and oxidation occur within the same cell. The main disadvantage of this configuration is the possibility of re-oxidation of the reduced cathodic products at the anode and vice versa. This phenomenon can lead to a significant decrease in efficiency and difficulty in product separation.[58] The alternative design, shown in **Figure 5b**, is the so-called H-type cell, a two-chamber, three-electrode reaction cell suitable for experiments where the anode and cathode electrolytes are different or not suitable for mixing. We note that the H-type cell is the most commonly used configuration for obtaining quantitative data independent of events at the counter-electrode, such as CO2RR or NRR. The two compartments are connected through an ion exchange membrane (a glass frit). For a reduction reaction, the cathode compartment most often houses the reference and working electrodes, while the anode compartment hosts the counter-electrode. The reverse is true when studying an electrooxidation reaction. This configuration makes it easier to study the characteristics of each half-reaction separately and to predict the performance of the paired electrolysis, e.g. the possible limiting electrode for achieving a high current density compatible with mass production of an energy carrier such as H_2 at the cathode (j = 0.2-2 A cm^{-2}),[4] while the biomass substrate is selectively electrooxidized at the anode. However, controlling the potentials applied to both cathode and anode is challenging.[59] The design of the three-electrode flow cell (**Figure 5c**) allows a uniform distribution of potential, reactant(s), intermediate(s), and product(s) over the working electrode surface and reduces the ohmic loss by keeping the work and counter electrodes close and parallel. In fact, the reference electrode is inserted close to the working electrode to control or to record the potential and minimize the solution resistance between both electrodes. Accordingly, such a design makes it possible to have a large working electrode and a small electrolyte volume, that is, a higher surface-to-volume ratio (S/V), which improves the efficiency.[55,60,61] We note that flow micro-reactors also increase the surface-to-volume ratio and enable forced convection, which reduces the diffusion layer thickness, which increases the mass transport limited current density (j_{lim}) according to Equation (2).[55]

$$j_{lim} = \frac{nSCFD}{\delta} \tag{2}$$

where:

δ: diffusion layer thickness,

n: theoretical moles of electrons (or number of electrons) transferred per reactant molecule,

F: Faraday constant,

S: electrode area,

D: diffusion coefficient,

C: bulk concentration.

The membrane electrode assembly (MEA) based flow cell design has a sandwich-like structure (**Figure 5d**), small reference electrodes can be inserted into each compartment to monitor the individual electrode potentials. We note that given the high input impedance of the reference electrodes, from 10^6 Ω to 10^{12} Ω, the porting of the current passing through a reference electrode (10^{-6}-10^{-12} A range) can be negligible when the electrolysis cell is operating at milliampere-ampere level current. Furthermore, a membrane (an ion conductor) should separate the anodic and cathodic layers, allowing ions to pass through while blocking electrons and gases such as H_2 and O_2. A more detailed description of the 2 main membranes is given in section 2.3. This configuration further reduces ohmic losses, minimizing cell voltage and improving efficiency.[55,58]

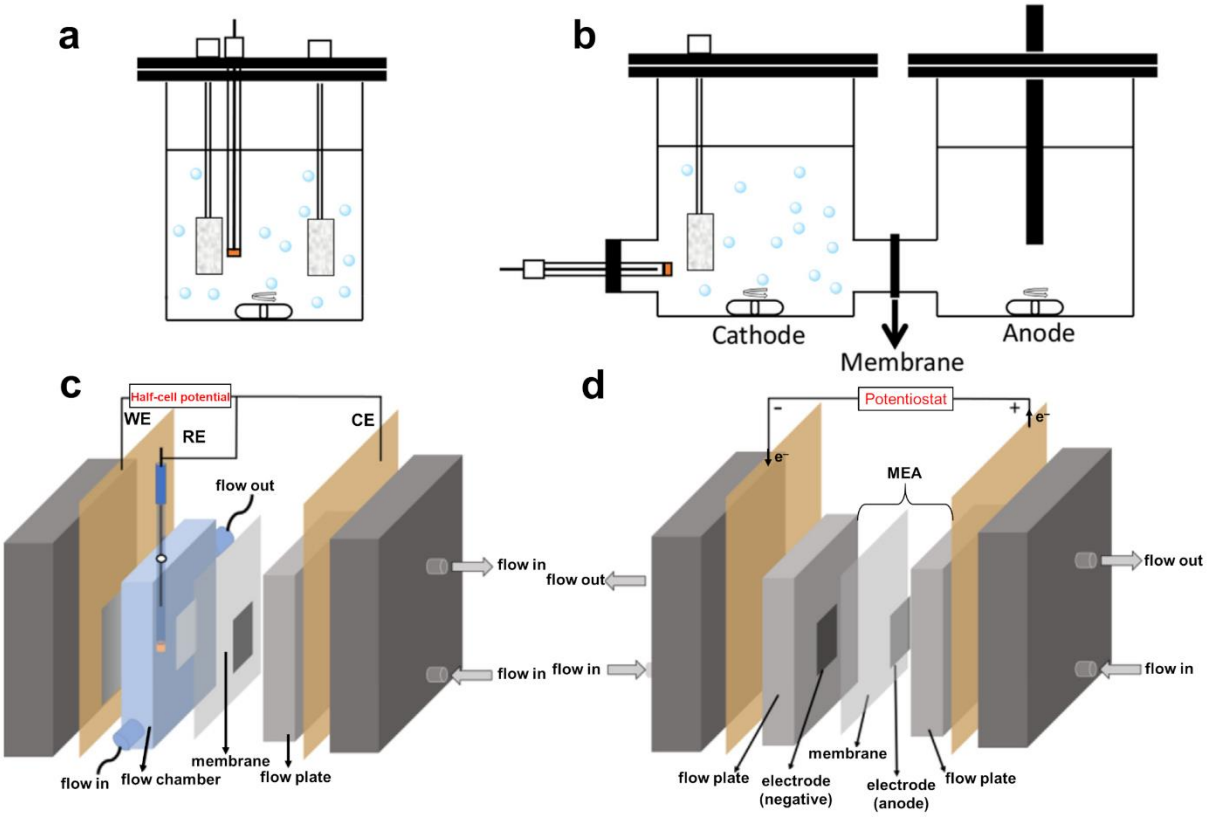

Figure 5. Schematic illustration of electrochemical cells as, a-b) Batch, and c-d) Flow. a) Single compartment batch cell. b) Two-compartment (H-type) cell. c) Three-electrode based flow cell with a spacer. d) Zero gap flow cell (MEA: membrane-electrode-assembly) under two-electrode

configuration. Reprinted and adapted with permission from ref.[58], Copyright 2021, Elsevier B.V.

2.1. Cathode compartment of an electrolysis cell

The cathode compartment of an electrolysis cell is one of the two main sections of the cell. This is the electrode where the reduction reaction takes place. As shown in **Figure 3**, the minimum energy input to operate an electrolysis cell must be equal to or greater than the potential difference between the anode and cathode compartments. Therefore, it is important to combine a reduction reaction with a thermodynamically favorable oxidation reaction to reduce the applied potential and consequently the energy consumption. Efficiency depends on three concepts to understand and optimize electrochemical systems:[55,62] the current density (*j*, A cm^{-2}), the overpotential (η, V) and the Faradaic efficiency (FE, %). Basically, *j* refers to the amount of electric current flowing through a unit area of an electrode. In the final electrochemical system shown in **Figure 5d**, the same current, algebraically of opposite sign, flows at the anode and cathode. This measurement helps to quantify the intensity of the electrical activity. It is therefore crucial to maximize the current per unit area in order to achieve a higher rate of product or reactant conversion, as electric current allows paired electrolysis processes to occur faster (Faraday's law), which can ultimately save costs and resources, but is the pinnacle of mass production of sustainable energy carriers such as H_2 or NH_3. The overpotential (η) refers to the difference between the experimental potential observed for an electrochemical reaction and the thermodynamically predicted potential for the same reaction (Nernst relation). It is caused by various factors such as internal resistances associated with mass transfer (η_{mt}), ohmic losses (η_{ohm}), and activation barriers (η_{act}). The overpotential is the extra energy required to drive the reaction beyond thermodynamic expectations. This is an essential parameter, as high overpotentials increase operating costs, reduce yields and, if too high, could result in damage to electrocatalysts and catalyst supports alike. The faradaic efficiency (FE) is a measure used to assess the extent to which an electrochemical reaction produces the desired products and avoids side reactions. Faradaic efficiency is a ratio that compares the actual amount of desired product to the theoretical maximum amount that could be produced based on the total electrons introduced into the system (Faraday's law). It is an important metric because it is directly related to the yield of the final product and the overall efficiency of the process.

2.1.1. Hydrogen Evolution Reaction (HER)

HER could be coupled with the biomass electrooxidation to implement the paired electrosynthesis of commodity renewable chemicals and fuels. As a function of pH, the overall process is expressed by Equations (3-4).

$$2H^+ + 2e^- \rightarrow H_2 \text{ (acidic media, } E° = 0 \text{ V vs SHE)} \quad (3)$$

$$2H_2O + 2e^- \rightarrow H_2 + 2OH^- \text{ (alkaline media, } E° = -0.83 \text{ V vs SHE)} \quad (4)$$

Two fundamental mechanisms governing HER electrocatalysis are widely accepted: the Volmer-Heyrovsky mechanism and the Volmer-Tafel mechanism.[4,55,56,63] Both routes begin with the Volmer stage, during which an adsorbed H atom is formed at the catalyst site via an electron transfer from the electrode coupled with a proton from H_3O^+ in acidic media (Equation (5)) or H_2O in alkaline media (Equation (6)).

$$H^+ + e^- \rightarrow H^* \text{ (acidic media)} \quad (5)$$

$$H_2O + e^- \rightarrow OH^- + H^* \text{ (alkaline media)} \quad (6)$$

The Tafel step in the Volmer-Tafel mechanism is the same in acidic and alkaline media, two H* atoms on the electrode surface combine to form H_2. There is no electron transfer in this step, so it does not directly involve an increase in current, but the recombination of the two adsorbed protons will release active sites, which will inevitably lead to the formation of new adsorbed protons, and as seen in Equations (5-6), is a faradaic process, so a change in electric current. For the design principles of electrocatalysts, therefore, the electrode surface configuration must contain sufficiently close active sites, whereas in previous cases only one was required.

$$H^* + H^* \rightarrow H_2 \text{ (for both acidic and alkaline media)} \quad (7)$$

The Heyrovsky step consists of electrochemical desorption of hydrogen to produce H_2 as illustrated by Equations (8-9) as a function of electrolyte pH.

$$H^* + H^+ + e^- \rightarrow H_2 \text{ (acidic media)} \quad (8)$$

$$H^* + H_2O + e^- \rightarrow H_2 + OH^- \text{ (alkaline media)} \quad (9)$$

Research on HER electrocatalysts for hydrogen production is intensifying. In general, precious metals including Pt, Pd, Ir, Ru and Rh serve as catalysts for this reaction, as they can

provide high active sites with appropriate binding energy for hydrogen adsorption.[64-73] However, there is a significant cost barrier to using these electrocatalysts in commercial applications. Therefore, various strategies have been developed to limit the amount of noble metals used (nano-structuring, carbon as support material, shaping, alloying, core-shell structuring, heteroatom doping, defect introduction and decoration, single atom catalysis, high entropy alloying, etc.).[74-87] The alternative approach is the non-precious metals for implementation in alkaline media because of the stability issues in acid electrolytes.[4,64,74,75,86-91] The most promising transition metals used in HER as electrocatalysts for alkaline water electrolysis (AWE) are Ni > Mo > Co > Fe > Cu. Seminal work by Nørskov *et al.*[92] has shown that transition metal carbides based on Ti, V, Mo, Ta and W can be potential substitutes for noble metal electrocatalysts due to their low cost, abundance and electrocatalytic properties. For HER, advances in the last decade have allowed the development of very low (a few micrograms of metal per square centimeter of electrode) non-precious metal electrocatalysts with overpotentials ranging from a few tens to a few hundred mV (E = 0.05-0.3 V vs RHE for j = 0.1-2 A cm^{-2}). To actually produce H_2 to meet the demand of millions of tons per year, the challenge lies in the anode, as OER requires more energy (E = 1.5-2.5 V vs RHE for j = 0.1-2 A cm^{-2}), which justifies the exponential increase in research devoted to the electrooxidation of organic molecules instead of water at the anode (**Figure 3**, Section 3).

2.1.2. CO_2 Reduction Reaction (CO2RR)

The conversion of CO_2 into valuable chemicals is a major innovation to achieve carbon neutrality, knowing that it is one of the main greenhouse gases responsible for climate change. In this context, electrochemical processes should play a central role to mitigate temperature increases while reducing CO_2 emissions. One of the most promising technologies is the electrocatalytic conversion of CO_2 into high-value products to produce low-carbon fuels and chemicals of economic value from CO, syngas, methanol to ethylene.[38,62,93-96] Meanwhile, formic acid stands as a safe and environmentally-friendly liquid H_2 carrier for the hydrogen bioeconomy. However, due to the highest oxidation state of the carbon atom (+IV) and its kinetic inertness (O=C=O), the CO_2 molecule is thermodynamically very stable. Consequently, a large amount of energy is required to activate it. Further, the energy of the molecule's C=O bond reaches 750 kJ mol^{-1} (>> C-H, C-C, C-O), which makes this conversion process very challenging. This process involves multi-proton-coupled electron transfer, especially for the production of more complex C2 and C3 molecules (alcohol, alkane, etc.).[67,97-102] In addition, a competing side reaction of HER with CO2RR occurs at the cathode due to their similar

potential values, which makes the production of the target product challenging. The selectivity and product distribution can vary significantly depending on factors such as the type of catalyst material, surface properties, reaction conditions (temperature, pressure, electrolyte composition, pH), and applied potential. Two common engineering approaches are aimed at improving the electrocatalytic performance (activity, selectivity and stability) of electrocatalysts: (i) increasing the number of active sites through better structuring of the electrocatalyst, (ii) enhancing the intrinsic activity per active site. It is known that the metal-CO bond strength, described as ΔH_{CO}, represents an important factor in the selection of a metal catalyst for electrocatalytic CO2RR.[67,101] The principle, known as the Sabatier principle,[103] emphasizes that metals with low CO binding energy (In, Sn, Pb, etc.) tend to facilitate formate production. On the other hand, metals with relatively low CO binding energy (Zn, Au and Ag) mainly yield CO. However, metals having too high a CO adsorption (Fe, Ni, Co and Pt) tend to poison electrocatalysts, thereby promoting HER. To catalyze the electrosynthesis of C2+ products, the only single metal electrocatalyst with high efficiency is Cu due to its moderate CO binding energy.[51,67,100,104]

2.1.3. N_2 Reduction Reaction (NRR)

Ammonia (NH_3) is a key feedstock in several industries: fertilizer, pharmaceutical and textile manufacturing. The Haber-Bosch process, which converts atmospheric N_2 into NH_3 for industrial use, is not only energy intensive (300-500 °C, 200-300 atm) and expensive, but also releases significant amounts of the greenhouse gas CO_2.[105-119] Electrochemical reduction of nitrogen (NRR) offers a sustainable alternative for NH_3 synthesis compared to the conventional Haber-Bosch process, but the reduction reaction still requires efficient catalysts to break the strong N≡N bond that has a dissociation energy of 941 kJ mol^{-1}.[108,120-123] Biomimicry, or biomimetism, is an approach to innovation and problem-solving that draws inspiration from natural processes to address issues by designing more sustainable, efficient, and innovative solutions to various challenges. For example, researchers have been inspired by the only enzyme capable of reducing nitrogen to ammonia, which is called nitrogenase. There are three main types of nitrogenase enzyme: MoFe, the most commonly used and most extensively studied nitrogenase, featuring an FeMo cofactor. There are also VFe and FeFe nitrogenases.[124-130] The choice of cofactors is made depending on the product being targeted (i.e., CO2RR, HER, NRR, etc.). Although biological nitrogenases have inspired the design of bioelectrodes for nitrogen fixation, many challenges remain, including the enhancement of the current density and stability of nitrogenase-based bioelectrodes.[131,132] Basically, it is postulated many types of

reaction mechanism for NRR.[108,117,132-135] However, since the activation barriers for Tafel-type reactions are around 1 eV or even larger for most transition metal based catalysts, the kinetics for a Tafel-type mechanism will be very slow. The process will therefore proceed via a Heyrovsky associative or dissociative reaction. The associative Heyrovsky mechanism, where N_2 molecules are hydrogenated by protons is illustrated by Equations (10-16), * = denotes the site.

$$* + N_2 \rightarrow *N_2 \quad (10)$$

$$*N_2 + (H^+ + e^-) \rightarrow *N_2H \quad (11)$$

$$*N_2H + (H^+ + e^-) \rightarrow *NNH_2 \quad (12)$$

$$*NNH_2 + (H^+ + e^-) \rightarrow *N + NH_3 \quad (13)$$

$$*N + (H^+ + e^-) \rightarrow *NH \quad (14)$$

$$*NH + 2(H^+ + e^-) \rightarrow *NH_2 \quad (15)$$

$$*NH_2 + (H^+ + e^-) \rightarrow *NH_3 \quad (16)$$

The Heyrovsky dissociative mechanism, whereby N_2 is initially dissociated at the catalyst surface and then hydrogenated is described by Equations (17-20).

$$2* + N_2 \rightarrow 2*N \quad (17)$$

$$2*N + 2(H^+ + e^-) \rightarrow 2*NH \quad (18)$$

$$2*NH + 2(H^+ + e^-) \rightarrow 2*NH_2 \quad (19)$$

$$2*NH_2 + 2(H^+ + e^-) \rightarrow 2*NH_3 \quad (20)$$

The Sabatier principle is a concept that describes the optimal conditions for a catalytic reaction to efficiently convert reactants into products. The implementation for NRR results into the N* binding energy as the performance descriptor at catalytic surfaces.[67,117,133,134] Metals having a strong bond of adsorbed N (left side of the volcano peak) lead to lower NH_3 production rates because of slow NH formation while metals having a weak interaction with catalytic surface (right side of the volcano peak) are constrained by the N_2 activation step. Pioneering theoretical calculations of NRR efficiency on transition metal electrocatalysts suggest that Mo, Fe, Rh, and Ru have the optimal binding energy, but the competitive HER reduces the faradaic efficiency for ammonia production.[103]

2.1.4. Nitrate Reduction Reaction (NO_3^-RR)

With the development of industrial and agricultural activities, nitrogen fertilizers have been overused, resulting in significant nitrate contamination of groundwater. This not only disrupts the natural nitrogen cycle, but also poses a threat to human health. Electrocatalytic nitrate reduction is one of the most commonly accepted methods for treating nitrates, and has attracted a great deal of interest due to its low cost, high efficiency and sustainable characteristics. Six products (NO_2^-, N_2, NH_3, NH_2OH, N_2O, and NO) can be obtained from electrocatalytic nitrate reduction. In order to produce a specific product, the selection of an appropriate electrocatalytic material and the incorporation of electrolyte must be considered to minimized the concomitant HER.[93,136-139] Current research is exploring different electrolytes, from aqueous (acidic, neutral, alkaline) to non-aqueous (ionic liquids, organic), which complicates the search for reaction intermediates and catalytic active sites. Compared to the NRR, the current densities and the NH_3 productivity of the NO_3^-RR are several orders of magnitude higher.

2.2. Anode compartment of an electrolysis cell

The anode compartment of an electrolysis cell is where the oxidation reaction takes place. The typical reaction is OER, which features prominently in many electrochemical conversion processes ranging from water splitting to CO_2 electrolysis. The overall reaction involves the oxidation of either water molecules or hydroxide ions to produce O_2 according to Equations (21-22).

$$4OH^- \rightarrow 2H_2O + O_2 + 4e^- \text{ (alkaline media, } E°\text{(V vs SHE) = 0.40)} \quad (21)$$

$$2H_2O \rightarrow 4H^+ + O_2 + 4e^- \text{ (acidic media, } E°\text{(V vs SHE) = 1.23)} \quad (22)$$

To date, the mechanism of OER is still debated, since it is very challenging to detect the majority of intermediates directly in experiments. From a computational perspective, OER routes are commonly represented by Equation (22-25) in acidic media and Equations (25-29) in alkaline media,[64,67,140] wherein * denotes the active site.

$$H_2O \rightarrow HO^* + (H^+ + e^-) \quad (23)$$

$$HO^* \rightarrow O^* + (H^+ + e^-) \quad (24)$$

$$O^* + H_2O \rightarrow HOO^* + (H^+ + e^-) \quad (24)$$

$$OO^* \rightarrow O_2 + (H^+ + e^-) \quad (25)$$

$$OH^- \rightarrow HO^* + e^- \quad (26)$$

$$HO^* + OH^- \rightarrow O^* + H_2O + e^- \quad (27)$$

$$O^* + OH^- \rightarrow HOO^* + e^- \quad (28)$$

$$HOO^* + OH^- \rightarrow O_2 + H_2O + e^- \quad (29)$$

OER suffers from a rather high overpotential due to its slow reaction kinetics, making it a challenging reaction to catalyze efficiently. As a result, it often requires the use of high performance electrocatalysts to overcome the energy barrier. In fact, carbon-based electrocatalysts are often oxidized, which remains a major challenge in this field.[141] In acidic media, noble metal oxide catalysts (IrO_2, RuO_2) demonstrate the most effective OER activity. Nevertheless, their limited availability and high cost hamper their widespread deployment. First row metals such as manganese oxides (MnO_x) have emerged for the development of OER catalysts due to their stability in alkaline conditions. The addition of Au to MnO_x has been shown to substantially augment OER activity.[142] In alkaline media, the OER can be efficiently catalyzed by inexpensive base metal oxides, oxy-hydroxides, sulfides, phosphides, etc.[4,64,67,87,143-149] Conclusively, the slow kinetics of OER impede the overall performance of water electrolysis. This reaction is both thermodynamically and kinetically unfavorable and produces O_2 of low value, until now. Therefore, a replacement for this reaction could be the biomass oxidation reaction, which can produce value-added products. Due to their low oxidation potential compared to OER, biomass-fed electrolyzers should require a lower cell voltage (*U*) than conventional electrolyzers. In Section 3.3, we will discuss the key points of electrooxidation of different biomass subunits.

2.3. Membranes

As water is a poor conductor of ions, a conductive electrolyte is required, whether in the form of a water additive or a solid electrolyte, for carrying out the electrolysis process at an acceptable cell voltage and current density (see **Figure 1**). Although historically used in alkaline water electrolysis (AWE), it is worth noting that other ionic conductors, such as inorganic porous separators impregnated with the liquid electrolyte, can result in high ohmic resistance and mixing between H_2 and O_2 gas, leading to some adverse consequences in terms of safety and gas purity.[4,64] The electrolyte itself should not be altered during electrolysis. Among the various electrolyzers types, hydroxide anion exchange membrane (AEM) and proton exchange membrane (PEM) systems have reached an advanced commercial level for the hydrogen processing industry.

2.3.1. Hydroxide AEM

In general, AEMs and PEMs consist of a polymer backbone. Charged functional groups are attached to the polymer backbone to provide conductivity and selectivity. PEMs are composed of negatively charged groups in the form of $–SO_3^-$, $–COO^-$, and $–PO_3^{2-}$, which are attached to the polymer backbone and ideally only allow H^+ to pass through (as other cations could be exchanged). In contrast, hydroxide AEMs contain positively charged groups, like $–NR_3^+$, $–PR_3^+$, and $–SR_2^+$, which are attached to the polymer backbone and only let OH^- through (**Figure 6**).[150-154]

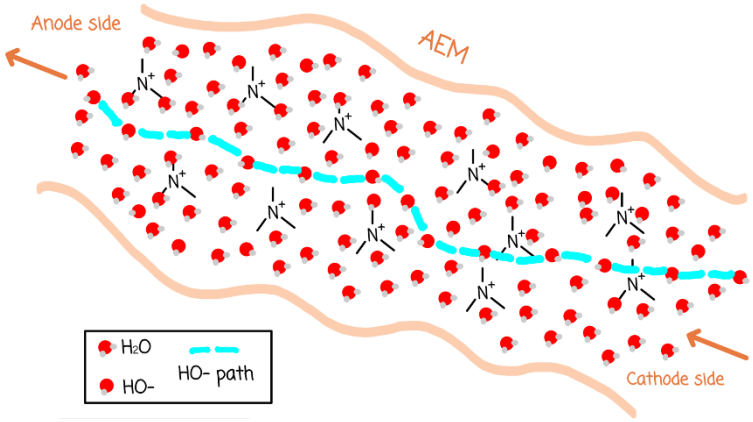

Figure 6. Illustration of hydroxide ions (OH^-) transport through a hydroxide AEM.

There are two main approaches that have been used to prepare AEMs. Each uses a different starting point to form the membrane:[150] (i) derived from the copolymerization of two functionalized monomers, and (ii) based on a preformed polymer film that is further modified by the introduction of positively charged functional units. The main criteria for the selection of an anion-conducting polymer membrane for use in an AEM electrolyzer are stability (chemical, mechanical and thermal stability), ionic conductivity and gas permeability. Chemical stability maintains a low degradation rate and good cell performance durability. The degradation rate of AEM was found to be affected by the concentration of HO^- and the temperature. The identified degradation mechanisms for the major functional groups are summarized in **Figure 7**.[4] A convenient ex-situ, reproducible technique for measuring AEM degradation has been reported for assessing the chemical stability of polymer backbones and their cation linkages in alkaline environments.[155] Excellent mechanical properties under practical operating conditions and thermal stability are required to ensure a long-term device. AEMs with a thickness of 40-50 μm are often manufactured, due to the limitations of the mechanical properties of polymer materials. To avoid mechanical failure of the membrane during cell operation, robust mechanical properties are required: >90% elongation at break, >15 MPa tensile strength, and a Young's

modulus between 75-400 MPa.[156-159] Several studies have shown that cross-linked membranes are successful in achieving the right balance between improved mechanical properties and low water swelling but good IEC.[154,160-163]

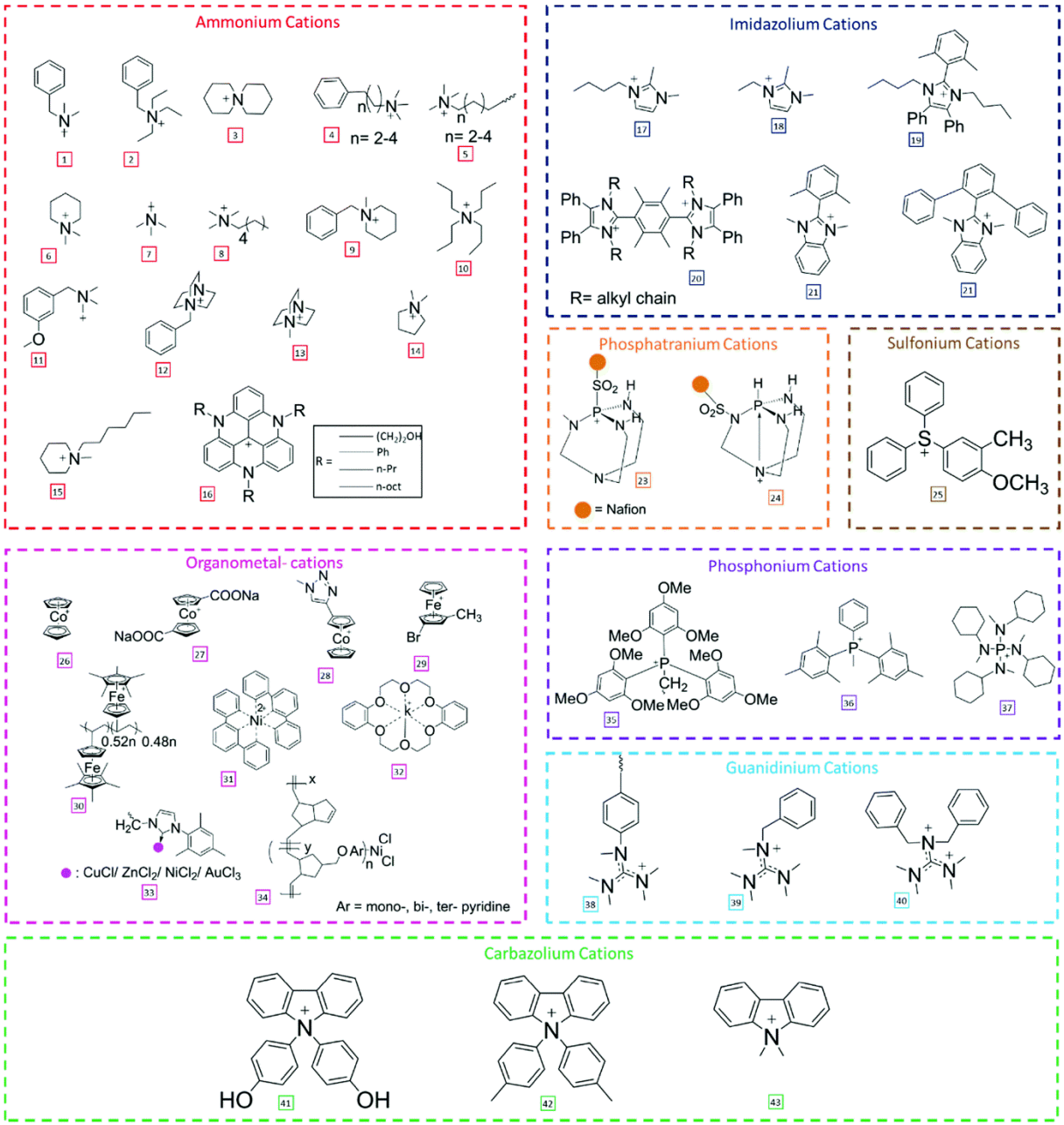

Figure 7. Schematic representation of typical cationic functional groups that are used in AEMs. Reproduced with permission from Ref.[4] under a CC BY 3.0 license, Copyright 2022, The Royal Society of Chemistry.

Other features of hydroxide AEMs include electrical insulation to prevent short circuits, extremely low gas permeability for preventing the passage of gas between the compartments, cost effectiveness, and high ionic conductivity (ideally, > 100 mS cm^{-1}) to transfer OH^- from the cathode to the anode. Although several commercial AEMs have been reported (**Figure 8**),

they are not as competitive in ionic conductivity as PEMs.[164,165] Nevertheless, AEMs with hydroxide ions conductivity exceeding 200 mS cm^{-1}[166,167] and operating continuously at measured temperatures close to 100 °C have been reported.[168,169] Higher hydroxide conductivity results principally from a high density of cationic functional groups, and hence a high ion exchange capacity (IEC). The majority of recently developed AEMs have a median IEC of 1.4-2.2 mmol g^{-1}.[4]

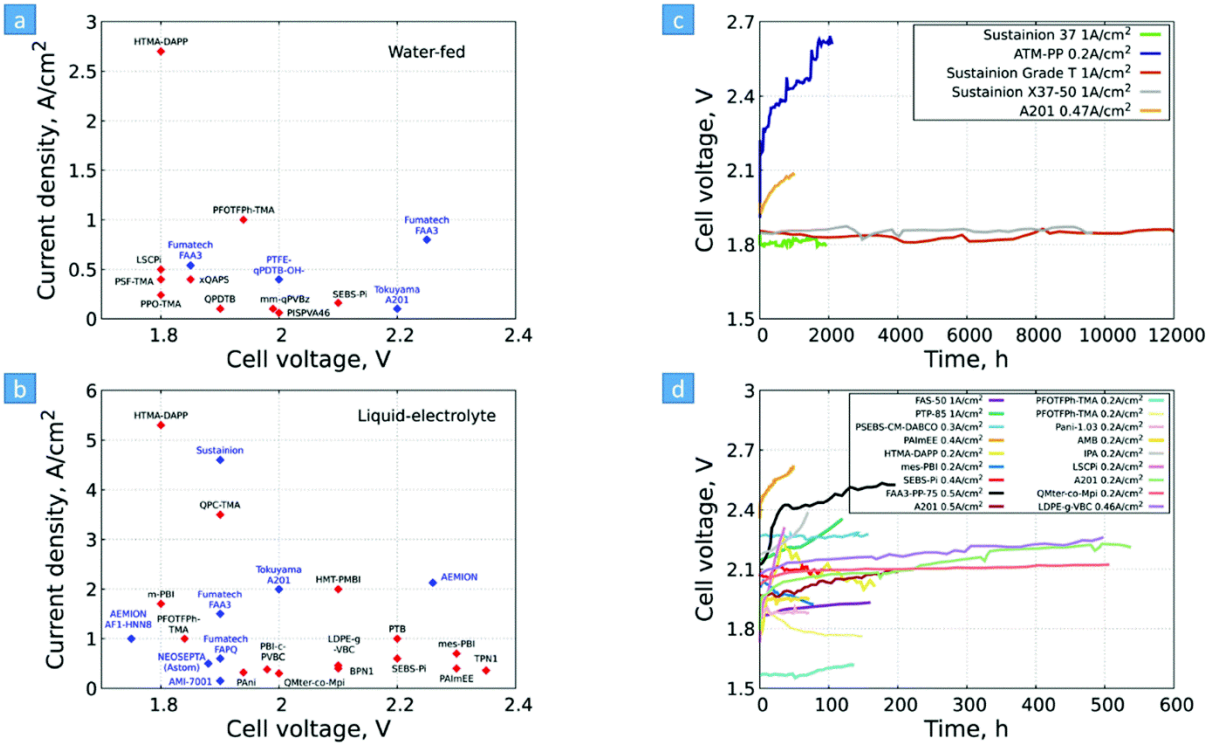

Figure 8. Performance of AEM-based water electrolysis. a-b) AEMs under development (university research, red boxes), and commercially available AEMs (bleu boxes) when the electrolyzer is fed by: a) pure water, and b) liquid electrolyte. c-d) Stability of selected AEMWE cells: c) long-term tests and d) short-term tests. Reproduced with permission from Ref.[4] under a CC BY 3.0 license, Copyright 2022, The Royal Society of Chemistry.

As far as ionic conductivity is concerned, some manufacturers measure hydroxide conductivity by soaking the membranes in a KOH or NaOH solution for complete ion exchange, before switching to pure water to remove excess base. This operation should be carried out in outgassed solution or in a glove box, to avoid any contact of the membrane with CO_2.[170] It is also possible to purge carbonates from the membrane by applying an electric current through it. The current causes electrochemical reactions, so that OH^- is formed at one electrode and HCO_3^-/CO_3^{2-} is drained off as CO_2 gas at the anode. It has been shown that the second method

gives better results and is more accurate with respect to the HO^- conductivity observed in an operating electrolysis cell compared to the first method.[171,172] A comparison of AEMWEs performance (cell voltage and current density) based on AEMs from research and industrial groups is reported in **Figure 8**. These data mostly highlight the excellent performance of the HTMA-DAPP AEM under development[173] and the commercially available Sustainion AEM. However, most AEMWE performance stability tests at constant current density revealed a loss of performance over the first operating 200 hours (**Figure 8d**). Only a few AEMs survive the performance test beyond 1000 h, such as Sustainion.[4,174,175]

2.3.1. PEM

During acid electrolysis, mobile proton species are trapped by the highly acidic polymer membrane. Therefore, PEMWEs require expensive and rare electrode materials that are resistant to such acidity. Modern PEMWEs feature significantly higher ionic conductivity (relative to AEMs), high mechanical strength, thermal resistance and chemical stability. Nafion membranes are the most widely used PEM materials, a type of perfluorinated sulfonic acid polymer that exhibits excellent proton conductivity. In fact, the higher the proton conductivity, the higher the current densities obtained.[4,176-179] Moreover, an advantage of these membranes is that they can be used as a thin layer (100-300 µm range) while maintaining good mechanical stability (low swelling, elastic), which allows the reduction of ohmic losses. However, the use of thin membranes increases the permeability of gases through the membrane, which is unsafe in these types of systems.[4]

Although PEMs are used in biomass-fueled electrolyzers, the majority of biomass substrates have a rather basic pKa between 10 and 13, meaning that AEMs would be best suited to paired electrosynthesis when biomass is considered. In fact, it is well known that the oxidation of organic substances involving coupled proton/electron steps, and therefore pH, has a key influence on the efficiency, as confirmed by fundamental studies which have shown that the efficiency is maximized at a pH close to the pKa of the compound because the alkoxide (dissociated anion) could be an active species.[13-15,52-54] One of the arguments for choosing PEMs was the unavailability of robust AEMs, but as mentioned above, R&D has progressed sufficiently in the last five years to offer efficient AEMs.

3. Electroconversion of Biomass-Based Chemicals in the Anode in Lieu of OER

3.1. Cellulose Structure

Lignocellulosic biomass, derived from plant matter (**Figure 9**), is mainly composed of 3 biopolymers cellulose, hemicellulose and lignin accounting for 30-40 wt%, 20-30 wt%, and 10-25 wt%, respectively.[42] Cellulose is actually a linear carbohydrate biopolymer built up from cellobiose monomers, each composed of two glucopyranose residues held together by β-1,4-glycosidic bonds. The cellulose polymerization degree (DP) ranges from 100 to 20,000, depending on the source.[180] In fact, these cellulose chains are stacked alongside each other to form microfibrils up to 3 nm thick in most plants, although in some algae they reach widths of over 20 nm.[181] Cellulose has a highly crystalline structure resulting from the formation of numerous strong intra- and inter-molecular H-bonds between hydroxyl groups.[182] The physical properties, such as the crystalline state, which depends on the arrangement of the glucan chains, and the molecular weight, which depends on the degree of polymerization, can vary significantly depending on the origin of the cellulose. Most cellulose found in natural sources is defined as cellulose I, which refers to a crystalline form of cellulose. Depending on the source of cellulose I, different amounts of two sub-allomorphic phases, Iα and Iβ, are found. The differences in molecular conformation and hydrogen bonding between cellulose Iα and cellulose Iβ result in different physical properties for cellulose microfibers.[183] Iβ of cellulose is thermodynamically more stable than Iα; note that the metastable Iα of cellulose can be transformed into Iβ by annealing at around 200°C in various solvents.[184,185]

In natural processes, the production of cellulose relies on the enzyme cellulose synthase, which uses UDP-glucose as a substrate. Whilst cellulose is one of the simplest polysaccharides known, its synthesis by non-enzymatic means is challenging. There are many reasons for the difficulty of synthesizing cellulose by non-biosynthetic routes, such as the need to perform regio- and stereo-selection at each step of monosaccharide subunit addition to regulate the relative direction (parallel or antiparallel) for each glucan chain. Actually, in cellulose, each glucose moiety is rotated or inverted by 180° vis-à-vis its neighbor. The β-1,4-linked glucan chains' insolubility and folding, which increase with the polymerization degree, also complicate synthesis.[183,186]

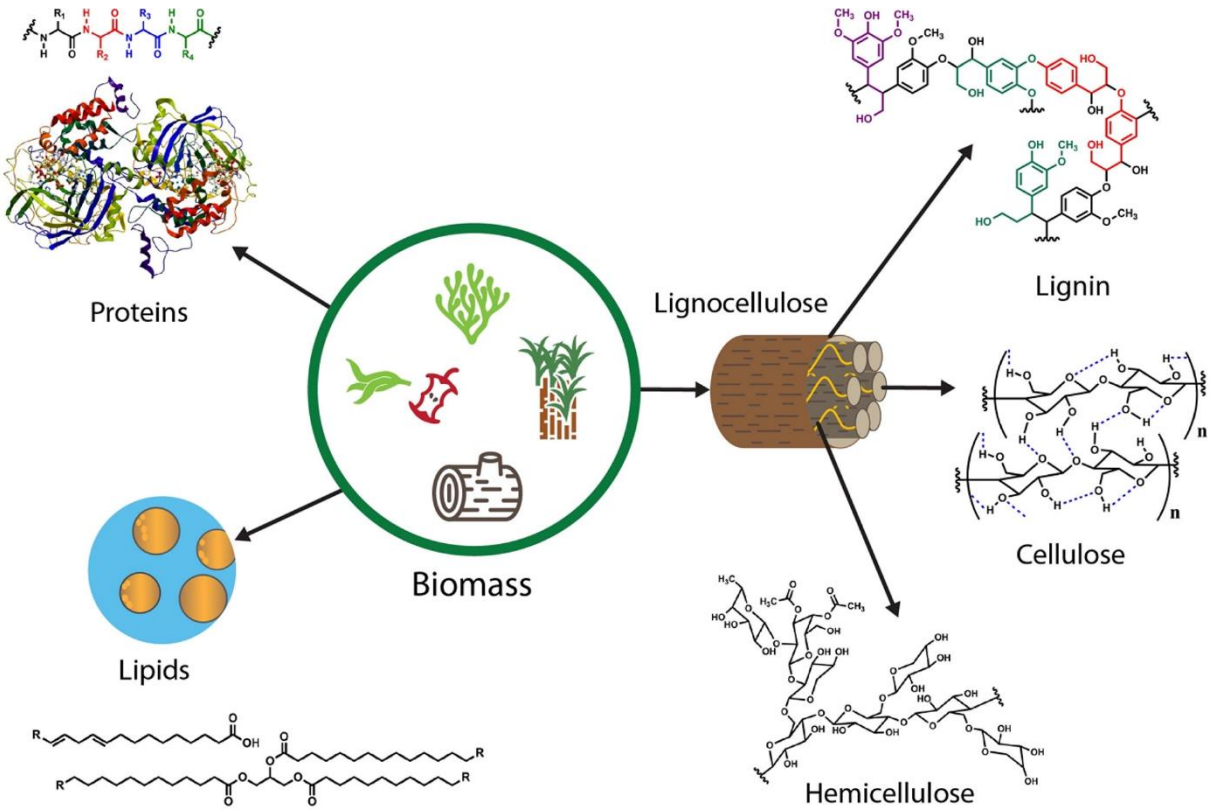

Figure 9. Biomass and lignocellulose derivates. Reproduced with permission from Ref.[42], Copyright 2021, American Chemical Society.

3.2. Cellulose Solubilization Methods

The cellulose abundance, its low oxidation potential (**Figure 1**), and the range of value-added products it can form make it an ideal candidate for electroconversion in a co-production electrolyzer. Nevertheless, the selective conversion of cellulose remains a major challenge due to its compact macromolecular structure. [187] Indeed, as seen above, the numerous strong intra- and inter-molecular H-bonds between hydroxyl groups (**Figure 10**) form an insoluble polymer in water as well as in most conventional solvents under normal conditions of temperature and pressure. In order to bring the active sites of the molecular chain into full contact with the electrocatalytic anode, it is essential to drastically weaken these H-bonds, resulting in the solubilization of the macromolecule.[180,188,189]

Yan *et al*.[190] have shown that dissolving cellulose in an alkaline aqueous solution facilitates the production of organic acids from malonic, lactic, formic and acetic acids. The study also identified cellulose concentration, reaction temperature and sodium hydroxide concentration as key parameters affecting the yield of the four organic acid types and the solubilization of cellulose. One of the methods developed for this purpose involves the use of

a concentrated aqueous NaOH solution at low temperature (0-4°C) for cellulose pretreatment, followed by a freeze-thaw process. The result is a nearly homogeneous solution. However, this method has its limitations because only low molecular weight cellulose can be dissolved in this solution. Therefore, the solubilization of cellulose is significantly improved by adding urea, an organic compound that can break the intermolecular hydrogen bonds of polysaccharides. In addition, urea optimizes the stability of the solution, which would otherwise form a gel at room temperature. The optimum condition to optimize solubility and stability of the cellulose suspension is an aqueous solution of 6 wt.% NaOH plus 4 wt.% urea.[191]

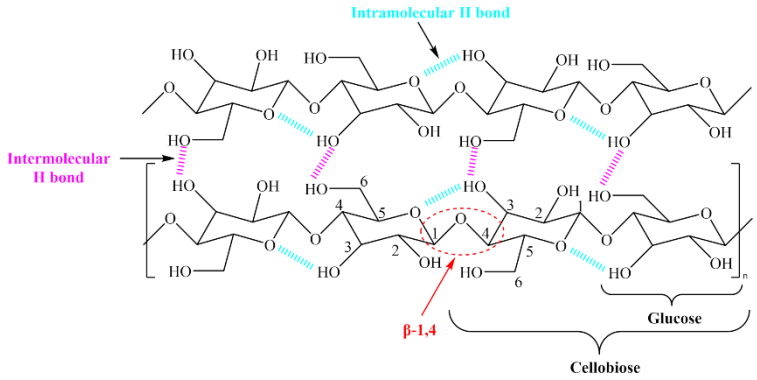

Figure 10. Structures and sub-units of cellulose (DP1: glucose, and DP2: cellobiose).

Two types of solvent are used for cellulose solubilization. One category of solvents transforms the cellulose into soluble derivatives during dissolution through chemical reaction with the cellulose (referred to as derivatizing solvents), whereas others are designed to preserve the cellulose's chemical composition (referred to as non-derivatizing solvents). For example, processes such as Viscose and CarbaCell or mixtures of organic and mineral acids rely on derivatization of cellulose.[180,192] However, ionic liquids (ILs) such as zinc chloride hydrate ($[Zn(OH_2)_6][ZnCl_4]$),[193] and some classes of imidazolium-based ILs,[194] or deep eutectic solvents (DESs) based on choline chloride,[195] appear to facilitate the conversion of cellulose into low-molecular-weight derivatives.

Dissolving cellulose depends on cracking the strong network of intermolecular and intramolecular hydrogen bonds present in cellulose, which ILs can do effectively. Clough *et al.*[196] have shown that mixing 1-ethyl-3-methylimidazolium carboxylate IL with carbohydrates such as cellulose leads to the formation of imidazolium adducts with a hydroxylated alkyl chain. The anions of ILs form hydrogen bonds with the hydroxyls of cellobiose, in one of two conformers (anti-anti and anti-syn). Therefore, since they play the main role in the dissolution mechanism, the modification of the ionic liquid cation could be

considered to avoid the formation of adducts. Indeed, the adduct-forming reaction mechanism for 1-ethyl-3-methylimidazolium acetate involves the C2 reactive position of the imidazolium ring. However, substituting this proton with a methyl group produces an IL with higher viscosity, a higher melting point and inferior thermal stability.[196] It has also been shown that the role of the cation in cellulose dissolution cannot be completely ignored. In fact, the cations present in the first coordination shell of cellobiose form hydrogen bonds with it.[197] On the other hand, anhydrous ionic liquids containing chloride anions appear to be the most effective solvents because of their ability to form hydrogen bonds with hydroxyl functions, thus separating the individual cellulose strands. They can therefore both dissolve cellulose and stave off an undesirable reaction of dialkylimidazolium cations with cellulose. For example, 1-butyl-3-methylimidazolium chloride has been identified as a sufficiently less reactive ionic liquid toward carbohydrates and can dissolve a significant amount of cellulose, especially when combined with microwave heating.[194,198,199] Several studies have also mentioned the depolymerization of cellulose in this type of solvent.[200,201]

The electrocatalytic oxidation reaction of biomass is being used primarily to replace the slow OER at the anode of an electrolyzer for H_2 production, with the aim of reducing the reaction voltage and improving efficiency. Currently, most of the world's chemicals originate from fossil raw materials, and chemical-producing industries are predominantly energy- and CO_2-intensive. Consequently, the electrocatalytic conversion of biomass feed-stocks is of great interest for research and applications. So, once the cellulose solubilization method has been perfected, the cellulose electrooxidation process can be considered. However, before undertaking this step, it is worthwhile to first examine the methodologies developed for the electroconversion of less complex organic compounds (e.g., HMF and glucose) derived from cellulose into value-added products, which are currently more effective.

3.3. Short chain Biomass-Based Substrate

3.3.1. Glucose

The elucidation of the selective electroconversion of the cellulose subunits (**Figure 10**) at high current density (and thus conversion rate) can serve as a model for further understanding of whole cellulose electrocatalysis. Glucose is the primary energy source for living organisms and the most abundant monosaccharide in nature. It is one of the derivatives of cellulose that can be obtained by its hydrolysis. The value-added chemicals that may be obtained from the electro-oxidation of glucose are gluconic acid (GNA), glucaric acid (GRA), glucuronic acid and formic acid. HMF, also resulting from the conversion of glucose, can be used to produce other value-

added products. For example, gluconic acid and its derivatives (gluconate, gluconolactone) are widely used in detergents, pharmaceuticals, agriculture, and as food additives. While glucaric acid and its derivatives have some interesting properties for healthcare.[202] Depending on the used catalysts and the reaction conditions, the reaction mechanisms and therefore the selectivity can differ significantly, leading to different products. Liu *et al*.[39] have designed two families of nanostructured catalysts, NiFe layered double hydroxide nanosheet arrays on Ni foams (NF) in the form of oxide (NiFeOx-NF, **Figure 11a-c**) and in the form of nitride (NiFeNx-NF, **Figure 11d-f**), which showed high activity and selectivity towards the anodic oxidation of glucose to glucaric acid (**Figure 11g**). The open fibrous structure and the electronic interaction between nickel and iron species contribute to the reduction of the charge transfer resistance, resulting at 1.3 V vs RHE, in a current density of 88 mA cm^{-2} (turnover frequency (TOF) value of 0.16 s^{-1}) for NiFeOx-NF, which is 4 times higher than NiFeNx-NF (22 mA cm^{-2} and TOF value of 0.04 s^{-1}).

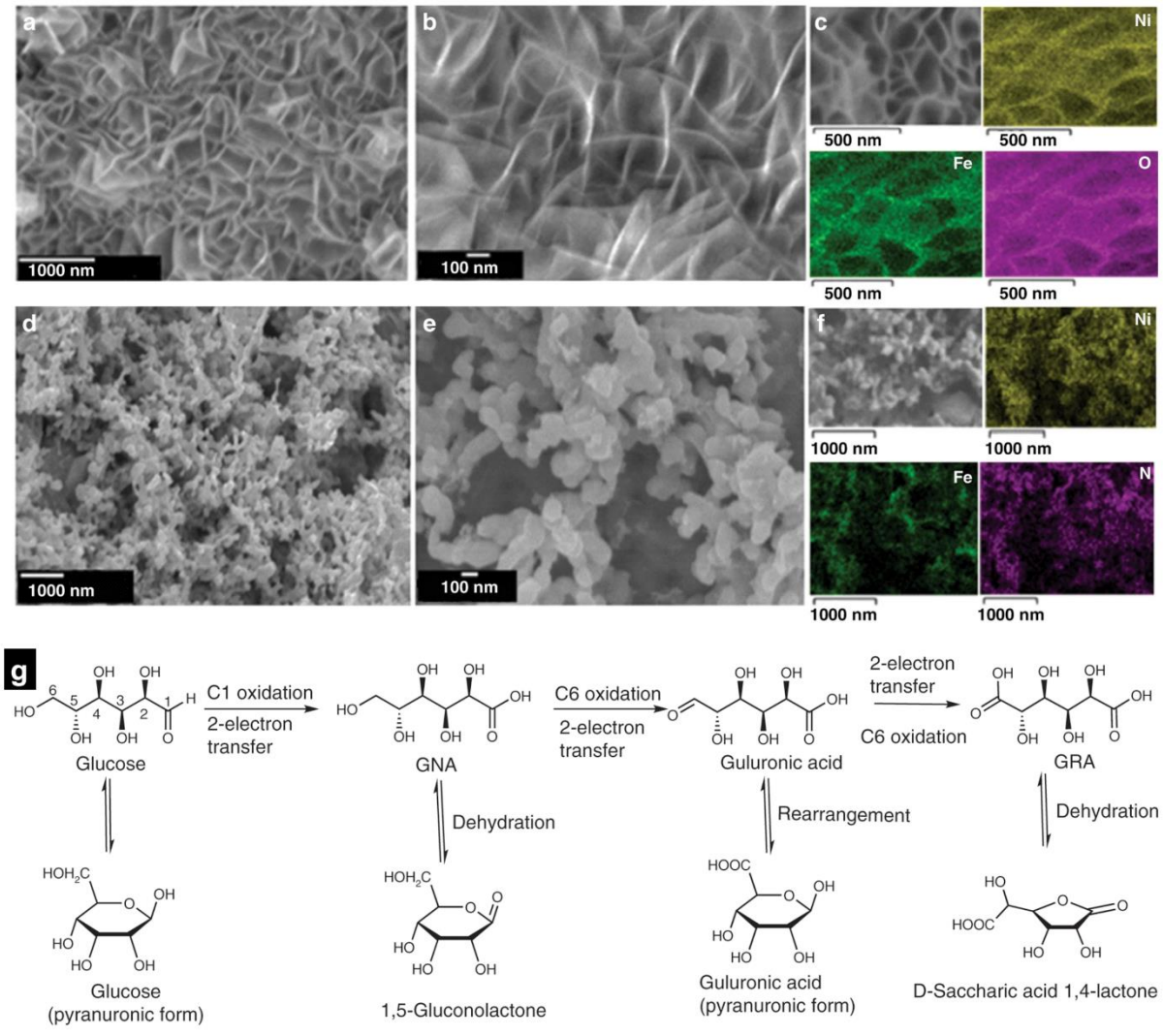

Figure 11. a-f) Noble metal-free electrocatalysts approach, bi-metallic particles synthesized onto a nickel foam (NF), SEM-EDS micrographs and elemental maps of: a-c) NiFeOx, and (d-f) NiFeOx-NF. g) Sketch of the main reactions occurring during the electrochemical oxidation of glucose, at NiFeOx-NF and NiFeNx-NF catalysts, to gluconic acid (GNA), guluronic acid and glucaric acid (GRA). Reprinted with permission from ref.[39] under a CC BY 4.0 license, Copyright 2019, The Author(s), published by Springer Nature Limited.

The potential-reactivity relationship of the functional group for the oxidation of glucose in alkaline media using 3 bare metal catalysts (Cu, Pt and Au) has been studied by Breugelmans *et al*.[203] On Cu, the reaction leads mainly to C-C cleavage products such as formic acid at high potentials. Besides, the oxidation of the C1 aldehyde group and the C6 hydroxymethyl group leads to modest efficiencies of gluconic and glucaric acid at lower potentials. The most significant process on Pt, both at high and low potentials, leads to a high selectivity towards gluconic acid. Au is the most active and selective electrocatalyst towards glucose electrooxidation. Like Pt, the main product obtained on Au is gluconic acid.[203] The overall mechanism as well as the possible in situ and ex situ methods for identifying reaction intermediates/products is shown in **Scheme 1**.

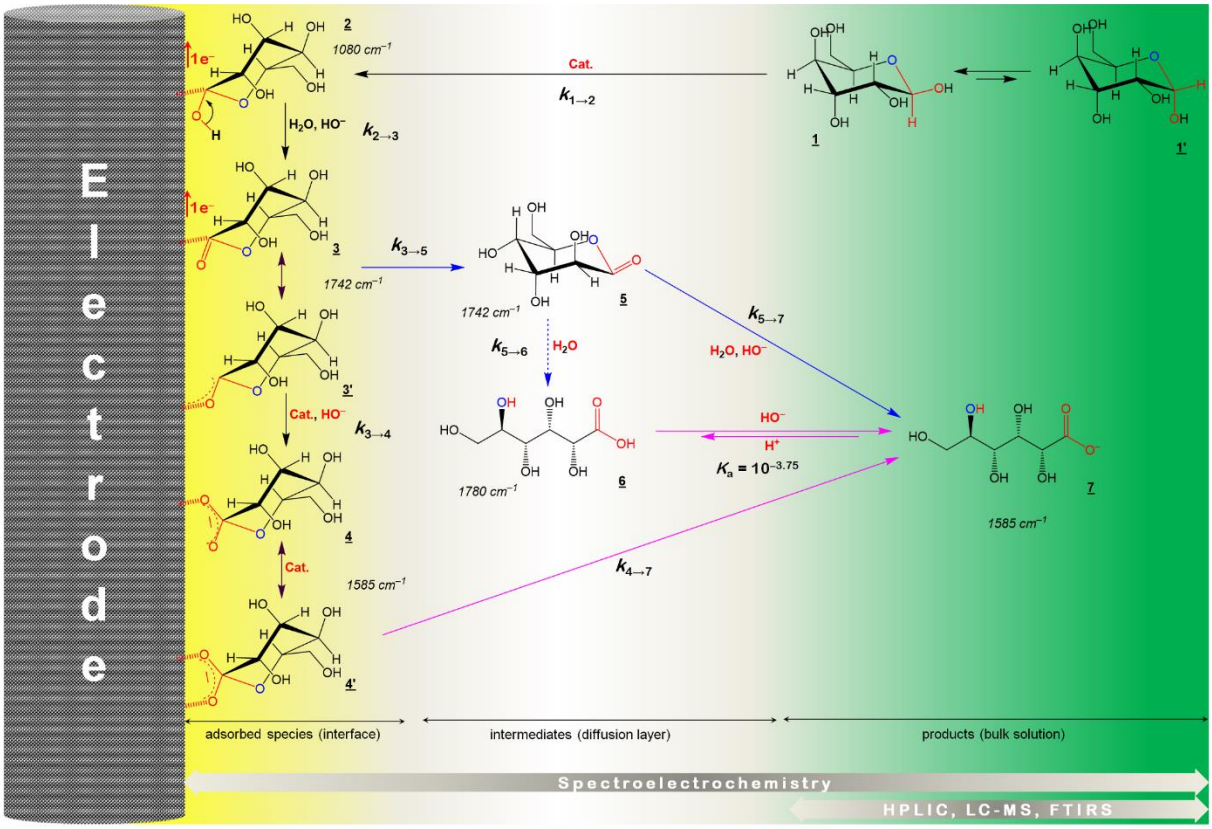

Scheme 1. Reaction scheme for glucose electrooxidation in aqueous media. Reprinted with permission from ref.[204] under a CC BY-NC-ND 4.0 license, Copyright 2018, The Author(s), Published by ECS.

To date, a wide range of different catalysts based on Pt,[205] Au,[206] Cu,[207] Fe,[208] Co,[209] and Ni[39] have been tested for electrochemical oxidation of glucose in alkaline medium. Among them, Au-based catalysts seem to exhibit one of the highest electrocatalytic activity, selectivity and stability below 1.2 V vs. RHE, because Pt rapidly deactivates and noble and non-noble metals require high potential (1.2-1.5 V vs. RHE), which breaks C-C bonds and increases the energy input. The cell voltage of an electrolysis cell is $U_{cell} = E_{(anode)} - E_{(cathode)}$ (Equation (1)) and the relation to the electrical energy consumed is given in **Figure 1**. Since the cathode potential for HER, CO2RR and NRR can be optimized to -0.1 to -0.5 V vs. RHE, the only approach to achieve low energy consumption is to keep E(anode) as low as possible. Therefore, in order to realize a non-exhaustive and efficient investigation of the best catalysts for glucose electrooxidation in alkaline media, our focus will be mainly on Au-based catalysts. Indeed, the support, the size, the shape and the crystallographic facets (*hkl*) of the electrocatalyst play a crucial role. Hebié *et al*.[210] demonstrated the size-dependent electrocatalytic activity of spherical Au nanoparticles. Electrocatalysts with smaller particles (4 nm and 6 nm) showed high catalytic activity for the electrooxidation of glucose in alkaline conditions. This drastic increase in activity compared to larger particles can be explained by the high specific surface area and surface electron reactivity induced by their small size. The intermediate and final products of glucose electrooxidation were determined to be gluconolactone and gluconate, respectively.[210]

Many synthesis methods have been developed to engineer gold-based nanoalloys[211-216] in order to increase the selectivity trends in electrocatalysis for electrolysis cells. Wang *et al*.[217] explored the catalytic activities of Au nanocrystals as a function of their shape for the electrooxidation of glucose in alkaline supporting electrolytes. It was shown that Au(100)-bounded cubic facets are known to exhibit higher activity than the Au(110)-bounded rhombic dodecahedral and Au (111)-bounded octahedral.[217] Arjona *et al*.[218] observed that Au(111) facets favored glucose byproduct oxidation while Au(200) facets favored glucose oxidation. They linked this behavior to the surface energy difference between the Au(111) and Au(200) structures. In fact, there is a higher affinity of Au(111) for the chemisorption of glucose molecules. As for Au(200), the affinity towards glucose by-products is weak, which allows their desorption, thus renewing the catalytic (metallic) surface for further electrooxidation of

fresh molecules of glucose.[218] **Figure 12** shows a series of results for both bulk gold electrode and nanostructured gold electrocatalysts for the oxidation of different forms of glucose at pH 7.4 (**Figure 12a-c**) and pH 12.8 (**Figure 12d-f**).[219] In fact, glucose ring closure by a hemiacetal bond results in a supplementary source of isomers on the anomeric carbon, termed α-D-glucose (the monomer unit of starch) and β-D-glucopyranose (the monomer unit of cellulose), where D-glucose forms a mixture of α-D and β-D.[220,221]

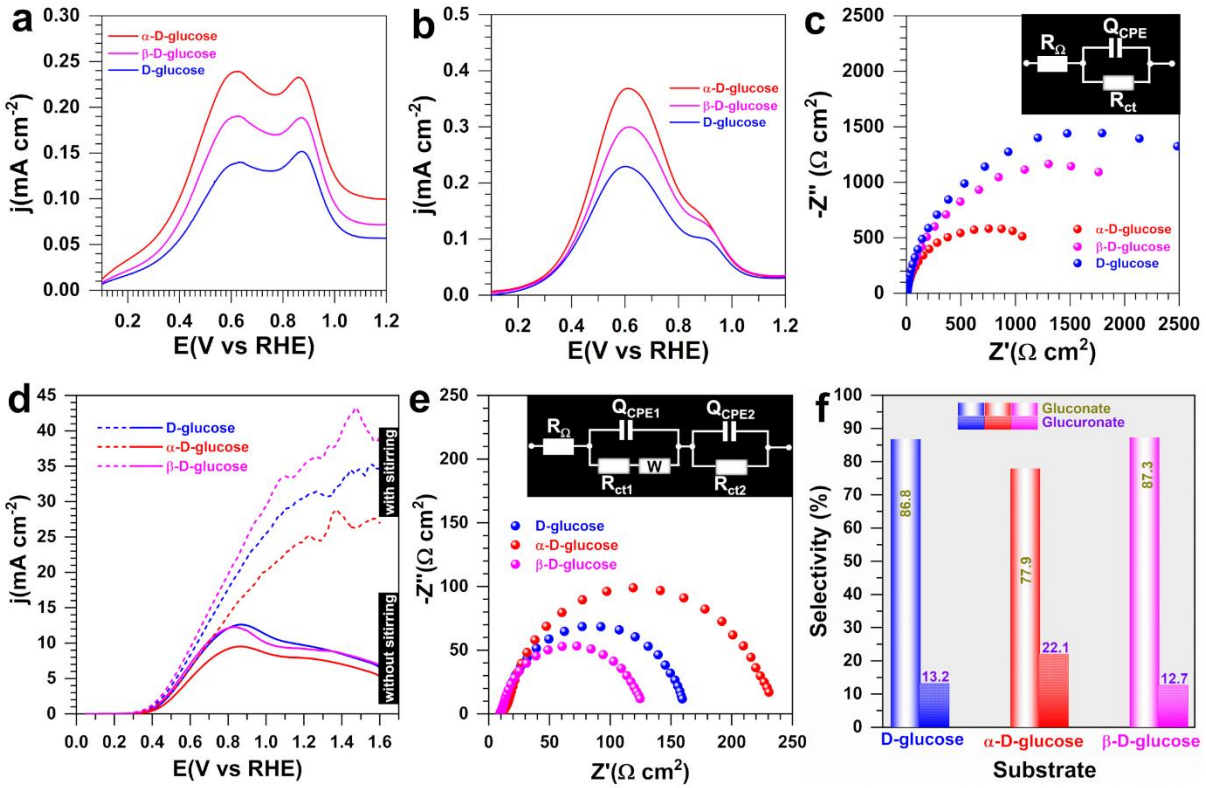

Figure 12. Effect of glucose type (D-, α-D-, and β-D-glucose) on the electrocatalytic performance in alkaline and neutral media at gold-based electrodes. a-b) Voltammograms [0.1 V s^{-1}, 0.2 M phosphate-buffered solution (PBS, pH7.4), 10 mM glucose, 25 °C] for D-, α-D-, and β-D-glucose: (a) electrochemically synthesized free-standing GDE-Au, and b) Au bulk. c) Electrochemical impedance spectroscopy (EIS) characterization by the Nyquist plots at 0.5 V vs RHE [Au bulk, 0.2 M PBS (pH7.4), 10 mM glucose, 25 °C]. d) Comparative voltammograms [GDE-Au, 0.1 V s^{-1}, 0.1 M NaOH (pH 12.8), 0.1 M glucose, 25 °C]. e) EIS characterization by the Nyquist plots at 0.34 V vs RHE [GDE-Au, 0.1 M NaOH (pH 12.8), 0.1 M glucose, 25 °C]. f) Products analysis after bulk electrolysis of [GDE-Au, 0.1 M NaOH (pH 12.8), 0.1 M glucose]. Reprinted with permission from ref.[219], Copyright 2022, American Chemical Society.

We note that D-glucose is the most commonly used in research, presumably because of cost since β-D-glucose is, respectively, 30 and 102 times more expensive than D-glucose and α-D-glucose. At neutral pH, the α-anomer has better electrocatalytic reactivity, while at alkaline pH, the β-anomer leads to the lowest charge transfer resistance. Energy profiles calculated as a function of potential using density functional theory (DFT) confirm the experimental results, suggesting that in the absence of hydroxyl functions on the gold surface, the hydroxyl group bonded to the anomeric carbon is deprotonated. In an alkaline electrolyte, the abundance of surrounding hydroxyl species near the metal surface triggers the dehydrogenation C–H of anomeric carbon (*β*-anomer) to generate an oxidized-type gold surface intermediate that is involved in the electrocatalysis of glucose.[222-225] The type of glucose substrate has minimal repercussions on the nature of the final product, which is gluconate with high selectivity and faradaic efficiency (>80%), meaning that both cellulose and starch could be used to fuel the cogeneration electrolyzer. Faverge *et al*.[226] have revealed by differential electrochemical mass spectrometry (DEMS) that, among Au, Pt and Pd, only Au allows the recombination of the adsorbed H (H_{ad}) to produce H_2 at low potentials range of 0.3-0.7 V vs RHE.

3.3.2. 5-Hydroxymethyl-2-Furfural (5-HMF)

Considerable efforts have been made in recent years to study the electro-valorization of biomass-derived compounds. Among hundreds of biomass-derived substrates, the electroconversion of 5-hydroxymethyl-2-furfural (HMF) has been the subject of intensive study. HMF is a furan compound obtainable directly from cellulose via a three-step reaction involving acid-catalyzed hydrolysis, isomerization and dehydration (**Scheme 2a**). HMF features a simple molecular structure comprising a furan ring, an aldehyde group and a hydroxyl group. Owing to its specific structure, there are fewer electro-oxidation selectivity problems with HMF than with other biomass derivatives, and it can produce a wide range of important chemicals, in particular 2,5-diformylfuran (DFF), 5-hydroxymethyl-2-furancarboxylic acid (HMFCA), 5-formyl-2-furancarboxylic acid (FFCA), and 2,5-furandicarboxylic acid (FDCA), which are shown in **Scheme 2b**.[227] Among these furan-based chemicals, FDCA is arguably one of the most desirable products of oxidation, as it is a renewable chemical building block with potential applications in the production of bioplastics such as polyethylene furanoate (PEF), used as a promising emerging substitute for traditional petroleum-based polyethylene terephthalate (PET).[228] FDCA is listed by the US DOE as one of the top twelve priority chemicals for building the green chemical industry of the future.[229] HMF's theoretical oxidation potential to FDCA is calculated at 0.3 V vs RHE,[230] which is considerably lower than OER's potential

(1.23 V vs RHE). Consequently, the electro-oxidation of HMF has attracted tremendous interest in order to improve the kinetics of this proton-coupled electron transfer (PCET) process, which is either HMF + $2H_2O \rightarrow$ FDCA + $6H^+$ + $6e^-$ (acidic media) or HMF + $6OH^- \rightarrow$ FDCA + $4H_2O$ + $6e^-$ (alkaline media). We note that the reader can refer to ref.[230] for standard half-cell potentials (anode and cathode) involving the electroconversion of HMF under different electrolytic conditions.

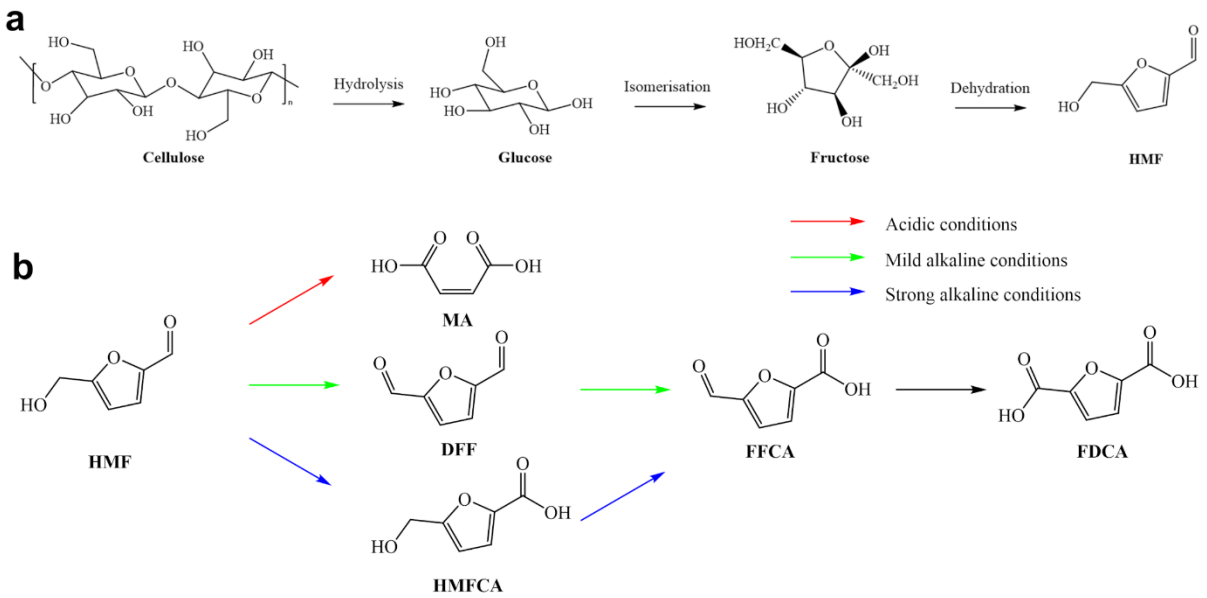

Scheme 2. a) Reaction pathways for HMF production from cellulose, and b) Overview of the electro-oxidation routes of HMF. Reprinted with permission from ref.[230] under a CC BY 4.0 license, Copyright 2023, The Author(s), published by Society of Chemical Industry and John Wiley & Sons Ltd, and from ref.,[227] Copyright 2021, The Royal Society of Chemistry.

The reaction pathway for the electrocatalytic oxidation of HMF has been investigated under different pH conditions, as illustrated in **Scheme 2b** Under mild alkaline conditions, HMF is initially oxidized to form DFF as primary intermediate.[227] Alternatively, highly alkaline conditions result in HMF being oxidized to HMFCA as the first intermediate.[230,231] DFF and HMFCA are then oxidized to FFCA, which is finally oxidized to FDCA. The degradation of HMF is an important issue in alkaline media where high current densities can be achieved. Nan *et al.*[232] have shown that HMF is more readily degraded at pH ≥ 12 and 0.1 M KOH seems to be the best compromise (**Figure 13a-b**). The debate concerns the stability of non-noble metal catalysts under oxidation conditions, since most non-noble metal catalysts, such as Cu-, Ni- or Co-based sulfides and phosphides, are susceptible to conversion to

oxides/hydroxides during oxidation (**Figure 13c-f**). Metal oxides may have a bright future in the electrochemical oxidation of organics, given the characteristics of their stable structure. Nevertheless, the poor conductivity and low active surface area of metal oxides, compared with the corresponding sulfides, phosphides, borides and nitrides, mean that they generally exhibit low electrocatalytic efficiency.

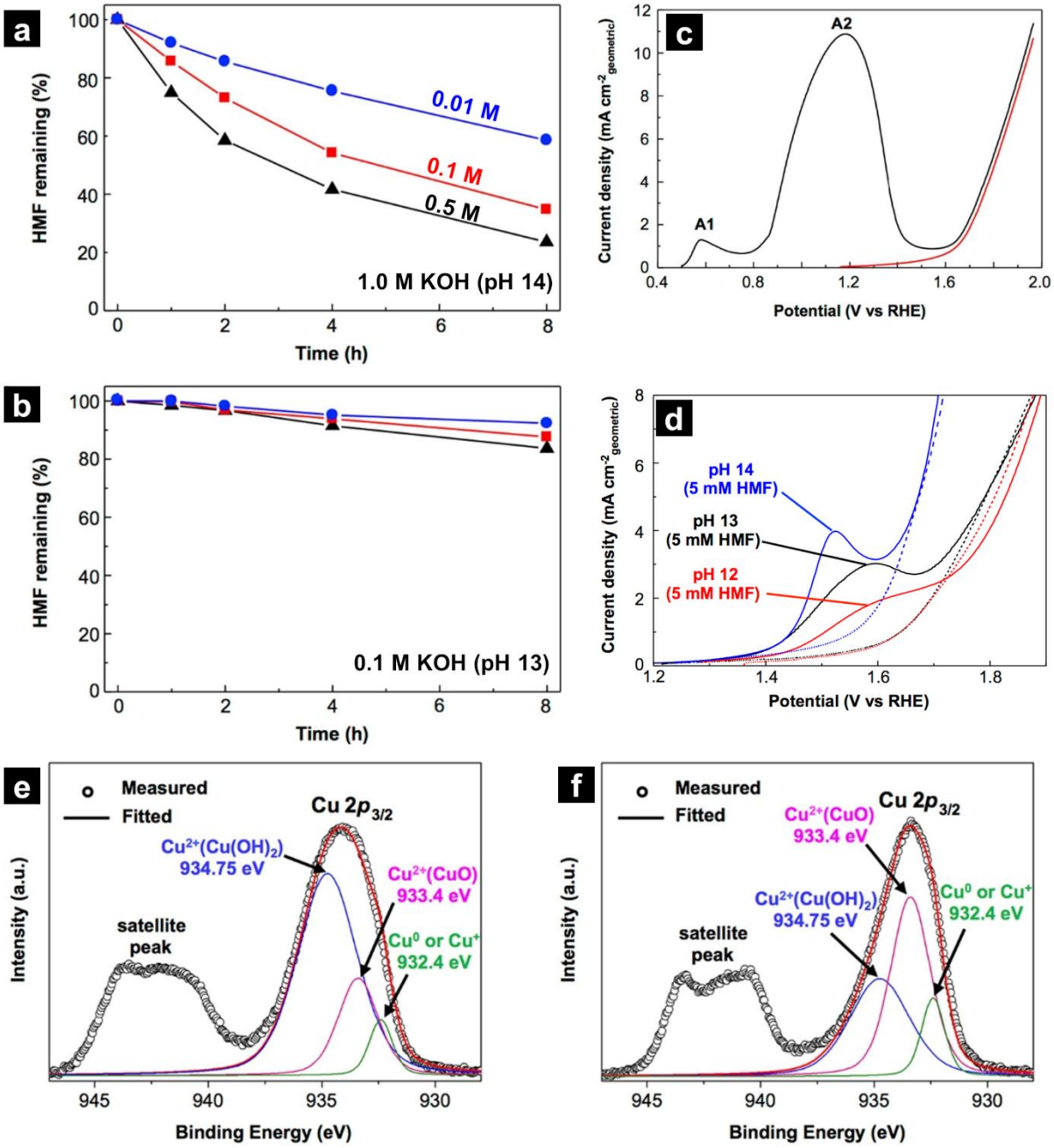

Figure 13. a-b) Effect of the concentration of the electrolyte [1.0 M KOH (pH 14) vs (b) 0.1 M KOH (pH 13)] on the chemical stability HMF [0.5 M (black triangles), 0.1 M (red squares), and 0.01 M (blue circles)] at room temperature under ambient pressure. Reprinted and adapted with permission from ref.[232], Copyright 2018, American Chemical Society.

HMF can generate maleic acid (MA) under acidic conditions and with a high applied potential. However, this is not desirable, as it consumes HMF and reduces the yield of FDCA.[233,234] Gao *et al*.[235] carried out electrochemical impedance analysis and electrolysis experiments, which showed that the electrocatalytic efficiency of their catalyst, TiOx-MnOx, hinges on HMF concentration. Other studies have shown that the electrolysis potential, reaction temperature and electrolyte concentration all play a role in the yield and faradic efficiency of FDCA.[235]

Currently, the main focus of the research teams for the electrooxidation of HMF to FDCA is the optimization of the electrocatalysts to further reduce the energy consumption and improve the yield. Controlling the kinetics of this process to achieve continuous oxidation while preserving the structure of the furan ring is the key issue. Therefore, catalytic systems with good selectivity have been developed. Metallic electrocatalysts can be classified into two main categories, depending on the materials used: noble metal catalysts and non-noble metal catalysts. Noble metals are known to be extremely active in a number of catalytic processes. When it comes to the selective electrooxidation of HMF to FDCA via DFF, noble metals with vacant *d*-electron orbitals, such as Au, Pt, Pd and Ru, have suitable surfaces for reaction contact and therefore perform very well.[40,44,236,237] For cost reasons, electrocatalysts based on non-noble metal-based like Fe, Co, Mn, Ni, and Cu have also been developed.[41,43,46,232,238-240] However, Pt, Au, or Pd are often added to increase the current density of the electrocatalysts at low electrode potentials, ideally below 1.2 V vs RHE, so as not to compete with OER and degradation of carbon-based substrates. Lu *et al*.[241] engineered a Ni nanosheet based electrocatalysts anchored vertically on a carbon substrate (Ni/CP) via an electrodeposition method for the electroconversion of HMF to FDCA. FDCA yields of >99% and H_2 faradic efficiencies of 95% at 1.36 V vs RHE. This enhanced catalytic activity and selectivity are ascribed to the nanosheet-like Ni species with a small crystal grain size, which preferentially transfer electrons to the semiconducting carbon scaffolds. Subsequently, electron-deficient Ni can be readily oxidized to $Ni^{\delta+}$ species and converted to NiO or NiOOH.

Yang et al.[242,243] have developed 3D electrocatalysts based on nickel foam to target both high current densities and high faradic efficiency for the selective electroconversion of HMF to FDCA. Specifically, Cr-$Ni(OH)_2$/NF with 1.4% Cr content led to $j > 0.36$ A cm^{-2} for the electrooxidation of HMF (20 mM) in an alkaline medium (1 M KOH), with 98% yield for FDCA. The reduction of Ni^{3+} to Ni^{2+} accompanied by the HMF dehydrogenation PCET process is the rate-limiting step that affects HMF electroconversion efficiency. Theoretical calculations

have shown that the PCET process on the Cr-doped NiOOH surface exhibits lower hydrogen transfer energy barriers, stronger covalent hybridization between metal sites and oxygen ligands with higher charge density, facilitating the capture of hydrogen protons from HMF molecules. Subsequently, the incorporation of P and Ru to synthesize PO_4/Ru-Ni$(OH)_2$/NF achieved the ampere-level current density suitable for industrial scale while using a proton transfer mediator for the electrooxidation of HMF to FDCA.[243] Specifically, the poised acceleration of the HMF dehydrogenation process (PCET) on the PO_4/Ru–Ni$(OH)_2$/NF surface led to remarkable performance for HMF electrooxidation at an industrial-level current density of 1-1.5 A cm^{-2} at 1.45-1.52 V vs RHE with high faradic efficiency (97%) and selectivity for FDCA (98%). DFT calculations confirmed the strategy of using a proton transfer mediator to accelerate the PCET process by lowering the energy barrier. In addition, simulations show that modifying Ni$(OH)_2$ with Ru can reduce the bandgap width, strengthen the Ni-O covalent interplay and enhance charge transfer. In addition, phosphate is capable of elongating the O-H bond of the HMF molecule, favoring its breakage to yield a moderate turnover frequency (TOF) of 0.05 s^{-1} at 1.45 V vs RHE for PO_4/Ru-Ni$(OH)_2$/NF (0.02 s^{-1} for Ni$(OH)_2$/NF),[243] which is presumably overestimated as only the available nickel-linked active sites were taken into account.

3.4. Electrocatalysis of Lignocellulosic Biomass

3.4.1. Cellobiose

Cellobiose is a disaccharide made up of two glucose molecules linked by a β-1,4 glycosidic bond, and is the smallest monomer making up cellulose. Morejón *et al*.[244] produced cellobionic acid from cellobiose by using a hypobromite/bromide redox couple as a mediator on graphite anodes in an undivided electrochemical cell. They achieved a 92% selectivity towards cellobionic acid and 48 % coulombic efficiency at 0.25 A cm^{-2} when using a charge of 2 FE (conditions: 0.25 M cellobiose, 0.25 M $CaCO_3$, 50 wt% $CaBr_2$, D_2O, 4 mL batch, 0 °C). Parpot *et al*.[26,245] achieved cellobiose oxidation in alkaline medium on gold catalyst. Following 20 hours of electrolysis, 95% of the starting cellobiose was converted to cellobionic acid. Small quantities of cellobiose dicarboxylic acid (3%) and traces of C-C bond cleavage were detected, thus confirming the high selectivity of the electrooxidation of the aldehyde/hemiacetal group without C-C bond cleavage.[26]

3.4.2. Long Chain Cellulose (DP >10)

Because of its complex chemical structure and insolubility in water, cellulose is less studied for direct electrocatalytic oxidation.[23,245-247] As noted above, cellulose's chemical structure is

relatively complex and insoluble in water, so the direct electro-conversion of cellulose into value-added chemicals has been the subject of sporadic study. Nevertheless, some works have investigated the electrooxidation of raw biomass. Hibino *et al.*[23] reported electrochemical hydrogen production from biomass wastes such as Journal newspaper, and rice chaff in an 85% H_3PO_4 solvent at high temperature (above 150 °C). They showed that cellulose and lignin can be hydrolyzed under these conditions at the anode into mono- and disaccharide derivatives and aliphatic molecules, respectively. A metal-free mesoporous carbon was used as the anode material. These biomass feed-stocks react ($(C_6H_{12}O_6)_n$) with H_2O to form protons and CO_2 at the anode, and H_2 at the cathode according to **Equations (30-31)**.

$$\text{Anode: } (C_6H_{12}O_6)_n + 6nH_2O \rightarrow 6nCO_2 + 24nH^+ + 24ne^- \quad (30)$$

$$\text{Cathode: } 2H^+ + 2e^- \rightarrow H_2 \quad (31)$$

Compared with the electrolysis of water and bioethanol, this approach offers greater savings in terms of the energy required to produce H_2. The average production was about 0.25 g H_2 per gram of biomass, nevertheless, the major drawback of this procedure is the CO_2 production at the anode.[248] Deng's group reported a process using polyoxometalates (POM $H_3PMo_{12}O_{40}$) as the catalyst and the electron-proton carrier for H_2 production and low molecular weight derivatives directly from native biomasses, such as cellulose and lignin.[249] In this process, the raw biomass was directly oxidized by the POM in the aqueous solution, but not at the surface of the anode electrode (homogeneous electrocatalysis). Electron transfer from biomass to POM could be enhanced by heating or solar irradiation. For reuse, the reduced POM was subsequently re-oxidized at the anode due to its low standard redox potential. During POM re-oxidation, H_2O is reduced at the cathode to produce H_2 (faradaic efficiency ~ 96%). POM has several advantages, it is recyclable up to 100,000 times, it requires a noble metal catalyst free anode, it is low cost and tolerates impurities generated by biomass. The electrolysis was performed at low temperature, at 0.2 A cm^{-2}, and with low electrical energy input (0.69 kWh per normal cubic meter of H_2), which is 6 times lower than for water electrolysis.[249]

Sugano *et al*.[22] investigated the dependence between the size and oxidation state of Au nanoparticles (AuNPs) based electrocatalysts and the electrooxidation of cellulose in alkaline media. Electrocatalytic activity in cellulose oxidation was found to be highest when Au NPs were smaller than 25 nm and when the oxidation state was 0. Zhao's group used Au nanoparticles supported by a carbon aerogel pretreated with HNO3 for the selective electroconversion of cellulose to gluconate in alkaline conditions.[250] After 18 hours of electrolysis, a high gluconate yield of 68% was achieved, which was attributed to the proper

dissolution of cellulose in NaOH solution, which favored its hydrolysis. In summary, very limited investigations have used gold-based electrodes for the electrocatalytic oxidation of cellulose or the indirect oxidation of cellulose as described above. Besides, the products of such systems have been difficult to identify and separate, making their practical application challenging.

3.4.3. Lignin

Next to cellulose, lignin is the second most abundant component of lignocellulosic biomass, and the largest source of renewable aromatic compounds. It therefore has great promise as a raw material for the production of aromatic chemicals.[251] However, the complex chemical structure of lignin makes it difficult to find selective catalysts to break it down into small molecules for fuel or chemical production. For this reason, research efforts have been stepped up to better understand the lignin oxidation mechanism (Scheme 3).[252] Stiefel *et al*.[253] studied a 3D-structured foam nickel electrode with a high active surface area that appeared to significantly enhance the lignin electro-depolymerization within a continuous reactor. Under room temperature and ambient pressure conditions, a molecular weight reduction of more than 93% was achieved in less than 4 hours. In addition, a nanofiltration membrane was coupled to the reactor to separate the low molecular weight compounds from the unreacted lignin, nearly tripling the concentration of value-added compounds. Among the products obtained by electrochemical cleavage of kraft lignin, phenolic monomeric compounds like vanillin, acetovanillone, carboxylic acids (e.g. phenanthrene carboxylic acid) and quinone compounds were identified. However, quantified individual compound yields did not exceed 0.5%, and no major products were identified.[253] The electrochemical degradation of corn stover lignin in alkaline electrolytes on Pb/PbO_2 based electrodes was investigated by Cai *et al*.[254] In the electrochemical oxidation process, minor lignin intermediates could be obtained after 2 h of electrolysis at 20 mA cm^{-2}, leading to 24 different types of compounds. The main valuable chemicals obtained were 4-methoxy-3-methyl-phenol (4%), trans-ferulic acid (2%), vanillin (1%), and syringaldehyde (1%).

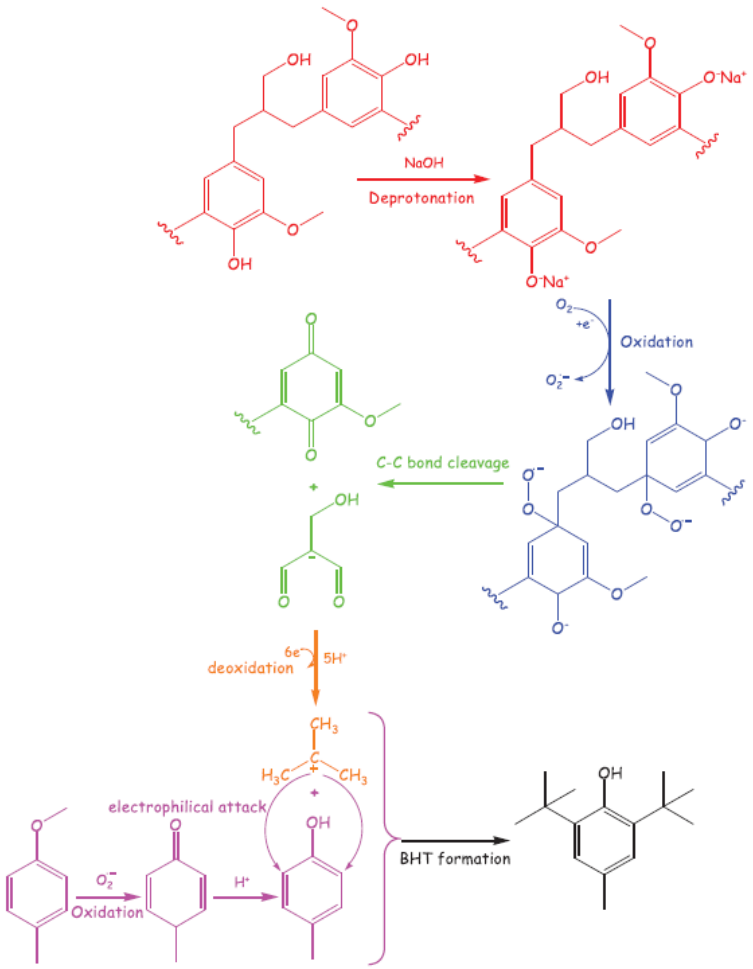

Scheme 3. Reaction pathways for the electrochemical oxidation of lignin to BHT (4-methoxy-3-methyl-phenol) on a Pb/PbO_2 electrode. Reproduced with permission from refs.[252,255], Copyright 2013, Society of Chemical Industry, and Copyright 2021, The Author(s), published by Wiley-VCH GmbH.

Garedew *et al*.[256] investigated how Ru catalyst supported on activated carbon cloth could be used to cleave 4-O-5 (ether) bonds while saturating the aromatic rings with hydrogen generated in situ. They selected dimer model compounds that exhibit this linkage. Both phenols, 3-phenoxyphenol and 4-phenoxyphenol, were cleaved to form cyclohexanol with 100% conversion. The cleavages of 3-phenoxyanisole and 3-phenoxytoluene were also completed, albeit with lower conversions and yields to cyclohexanol due to their limited solubility. The main mechanistic clues revealed are that oxygenated functional groups on aromatic rings adjacent to the ether bond tend to speed up cleavage, which may be due to electron-withdrawal effects that activate ether oxygen. It has been shown that by increasing the substrate concentration (from 10 mM to 40 mM), and especially by decreasing *j* from 33 to 7 mA cm^{-2}, the faradaic efficiency can be increased to 96% and the cyclohexanol yield to 87%.[256] In most

studies, modest yields of valuable chemicals such as vanillin or organic acids were obtained. Lignin polymer complexity is a major challenge for the development of electrocatalysts adapted to its conversion. In fact, its structure can hinder the access of the active electrode sites to the lignin bonds, which can hinder the selectivity towards a specific product. Therefore, selectivity remains a critical challenge to be overcome for lignin electrooxidation. A number of recent studies have introduced product separation systems, using nanofiltration membranes coupled to flow reactors, designed to address this problem.[257,258] Also, the limited solubility of lignin in solutions other than alkaline media limits the electrolytes that can be used during electrolysis, which can be challenging as the stability and activity of certain electrode materials may be compromised under alkaline conditions. However, ionic liquids and deep eutectic solvents appear to be a promising alternative to overcome the challenges associated with electrolyte limitations.[259]

4. Paired Electrosynthesis: Coupling Processes at Cathode and Anode

The electrolysis process involves the pairing of two half-reactions, oxidation at the anode and reduction at the cathode. In general, the reaction at one electrode tends to be more significant (valuable product) than that at the other. The best-known illustration is water electrolysis, where the cathodic HER, which produces green H_2, is more valuable than the anodic OER, which produces O2 (not yet considered a valuable product). In addition, the effectiveness of water splitting is hampered by OER's high activation barrier. Consequently, opting for a more thermodynamically favorable oxidation reaction by choosing one that occurs at minimum potential is an effective way of reducing the energy demand of the overall process, obtaining high-value products and avoiding the generation of explosive H_2-O_2 mixtures at high pressure. Here, the pairing of HER, CO2RR and NRR with biomass-derived oxidation reactions is reviewed. For paired electrolysis, where both reactions are delivering valuable chemicals, other factors need to be taken into account, such as complementarity, product compatibility and current matching. Furthermore, as we have seen in previous sections, the energy required to run paired electrolysis may be minimized by refining the parameters of each reaction. For instance, through adjusting electrolyte pH, temperature, pressure, electrode material, etc.[43]

4.1. Coupling Biomass Electrooxidation (Anode) with HER (Cathode)

To reduce the overall cost of the electrolysis process, the use of a bifunctional and bimetallic electrocatalyst can be an efficient strategy, which also synergistically increases the number of active sites, intrinsic activity, and stability. Lin *et al*.[145] used porous Co–Ni alloy on carbon

cloth in alkaline environment for both glucose electrooxidation and HER, which lead a decrease in the cell voltage of 0.26 V at 10 mA cm^{-2} and 1.39 V in KOH (1 M) + glucose (0.1 M) while KOH (1 M) leads to 1.65 V (H-type electrolysis cell). **Figure 14** represents the electrolyzer and economic analysis when the same type of NiFe-based electrocatalysts are used at the anode and cathode.[39] The advantage of using glucose is obvious with a current density of 0.1 A cm^{-2} at 1.39 V (FE of 87%; yield of 83% for glucaric acid (GRA)). It is interesting to note that the comparison of revenues and costs between electrocatalytic and non-electrocatalytic approach (HNO_3 oxidation) for GRA production highlights a 54% lower cost for the electrocatalytic approach. It should be noted, however, that for such porous electrodes (mostly metal foams), comparison with results from non-porous electrodes is problematic because the effective surface area is underestimated.[260]

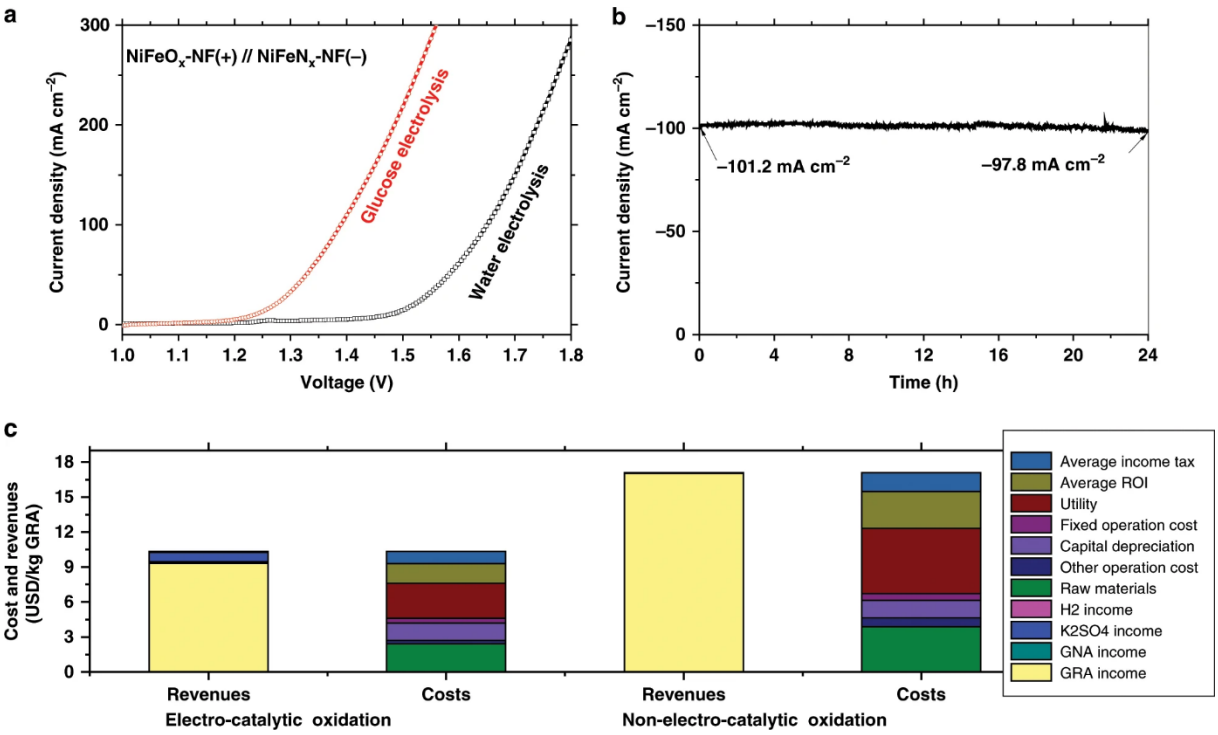

Figure 14. Performance and the economic feasibility of the glucose electroconversion. a) Polarization curves at 0.005 V s^{-1} [0.1 M glucose, 1 M KOH, two-electrode H-type electrochemical cell (anode: NiFeOx-NF, cathodic: NiFeNx-NF, hydroxide AEM: AMI-7001 (Membranes International Inc., USA)] for glucose electrolysis and water electrolysis. b) Corresponding stability of the glucose electrolysis at 1.4 V. c) Comparison of the revenues and costs of glucose oxidation processes: electrocatalytic and non-electrocatalytic oxidation (HNO_3 oxidation) for glucaric acid (GRA) production (1000 tons GRA per year). Reprinted with permission from ref.[39], Copyright 2019, The Author(s), published by Springer Nature Limited.

Among the many valuable products, the simultaneous production of 2-furoic acid and H_2 from the integrated oxidation of furfural (anode) and HER (cathode) is of great interest. Several catalysts have been developed for this coupled system. For example, furfural oxidation and H_2 evolution were investigated by Jiang *et al*.[261] using Ni_2P/Ni/NF as a low-cost bifunctional electrocatalyst. They achieved nearly 100% FE and 98% yield for 2-furoic acid under ambient conditions in alkaline media. Compared with the conventional water separation method, the cell voltage was decreased by ca. 0.1 V to achieve a current density of 10 mA cm^{-2}. In addition, maleic acid can also be produced as the main product from furfural on a PbO_2 anode when paired with HER in an acidic medium (pH 1.0, H_2SO_4) at ambient temperature and pressure without using oxidants. Using an acidic medium, to promote furan ring opening during oxidation, is essential for forming maleic acid.[262] Wang *et al*.[46] designed a paired electrosynthesis system combining furfural oxidation with HER at a low voltage of ~0.1 V vs. RHE. When assembled, the electrolyzer consumed just ~0.35 kWh of electricity per m^3 of H_2, whereas conventional water electrolysis requires ~5 kWh per m^3 of H_2. The combined EF was around 200%, with HMFCA being the main product on the anode.[46]

Like furfural, more progress has been made in HMF integrated with HER conversion system. You *et al*.[263] reported a hierarchical porous Ni_3S_2/Ni foam bifunctional electrocatalyst (Ni_3S_2/NF). HMF was oxidized to FDCA at much lower overpotentials than that of OER (reduced by ~200 mV to reach 100 mA cm^{-2}). When used as electrocatalysts for both cathode and anode, 100% conversion (HMF) and 98% FE (FDCA production) were achieved. Zhang *et al*.[264] also used a bifunctional non-noble metal-based catalyst. The carbon-coupled nickel nitride foil electrode (Ni3N@C) required an overpotential of 240 mV below OER, and the FDCA yield remained at 98% after six electrolytic cycles working with the same electrode. Shao's group reported an ultrathin CoAl-LDH nanosheet array (CoAl-LDH-NSA) for HMF electrooxidation to FDCA paired with H_2 production at a moderate potential (1.3 V vs RHE).[265] Benefiting from a considerably enlarged electrochemically active surface area and the presence of ample oxygen vacancies, ultrafine CoAl-LDH-NSA exhibits significantly improved H_2 and FDCA yields, with FE of nearly 100%. The H_2 yield was 4 times higher than overall water splitting (44.16 L h^{-1} m^{-2}) and 63.38 g h^{-1} m^{-2} of FDCA were obtained.[265] The same group designed a bifunctional CoNiP for both HER and HMF oxidation reaction. The cell voltage (1.46 V) was 300 mV lower than that of water splitting (1.76 V) and a 41.2 L h^{-1} m^{-2} production rate of H_2 and a 85.5 g h^{-1} m^{-2} yield of FDCA in alkaline electrolyte.[266]

For pairing biomass electrolysis with H_2 production by HER, the number of electrons necessary to form one molecule of H_2 ($H_2O + 2e^- \rightarrow H_2 + 2OH^-$) is two. As a result, if the

representative biomass is the electrooxidation of glucose into gluconate at the anode ($C_6H_{12}O_6$ + $3OH^- \rightarrow C_6H_{11}O_7^-$ + $2H_2O$ + $2e^-$) and HER at the cathode, only 2 electrons are required to convert 1 molecule of glucose into 1 molecule of glucose and 1 molecule of H_2 ($C_6H_{12}O_6$ + $OH^- \rightarrow C_6H_{11}O_7^-$ (anode) + H_2 (cathode)). In some cases, the anodic oxidation reaction of biomass may require a much higher number of electrons,[214] for example, the transformation of 1 molecule of 5-HMF (1 aldehyde function + 1 alcohol function) into 1 molecule of FDCA (2 carboxylic acid functions) requires 6 electrons.[267] Such PCET cascades[13-15] lead to kinetic bottlenecks in electron transfer and mass transport.

4.2. Coupling Biomass Electrooxidation (Anode) with N_2RR or NO_3^-RR (Cathode)

Another electrocatalytic reaction receiving recent emphasis is electrochemical NRR, which represents a potentially viable replacement for the traditional Haber-Bosch process. Only a few works have reported on the electrooxidation of HMF coupled with NRR. Yet, to minimize the high input voltage arising from kinetically slow OER at the anode, Ma et al. paired NRR with HMF oxidation by utilizing a bifunctional electrocatalyst, ruthenium(III) polyethyleneimine (Ru(III)-PEI), supported on carboxyl-modified carbon nanotubes (Ru(III)-PEI@MWCNTs). At -0.10 V vs RHE, the catalyst exhibited a yield of 189 μg_{NH3} mg_{cat}^{-1} h^{-1} for a FE of 31% at room temperature. The electrode showed a cell voltage 220 mV lower than that of OER. At U_{cell} = 1.34 V, j = 0.50 mA cm^{-2} during 27 h of stable electrolysis, which led to 94% FE for FDCA production.[268] Qin *et al*.[269] reported the use of N- and B-doped porous carbons for NRR and HMF electrooxidation. A maximum FE of 15% was obtained with a stable a productivity of 21 μg_{NH3} mg_{cat}^{-1} h^{-1}. On the other hand, FDCA is obtained with a conversion rate of 71% and a yield of 57%.[269]

4.3. Coupling Biomass Electrooxidation (Anode) with CO2RR (Cathode)

CO2RR can produce a variety of reaction products, including C1 products such as CO and HCOOH, which are obtained by a two-electron reduction process. The key factors governing product yield are the adsorption/desorption of CO_2 and any intermediates formed on the electrode surface. These factors are influenced by the catalyst design and electronic structure, the electrolyte, and the applied potential.[38,100,270] A techno-economic study performed by Verma *et al*.[37] suggested that provided total energy consumption (i.e. cell potential) can be significantly reduced, CO2RR with grid electricity could achieve carbon neutrality, making it economically feasible. Since approximately 90% of the total energy requirement (cell potential) is due to the oxygen evolution reaction (OER), the authors further investigated the economic

feasibility of coupling CO_2RR with various anode reactions that have a lower oxidation OER. These reactions include glycerol, glucose, and CH_4 electrooxidation, of which glycerol can reduce power consumption by up to 53%. According to these requirements that they stated for the anode reaction, electrochemical oxidation of HMF would be a perfect match. Not only does it have no CO_2 emission, but it also produces a high value-added chemical (FDCA). Therefore, the electro-oxidation of HMF could also be considered as a relevant anodic reaction to substitute OER and diminish overall cell voltage needed to run CO2RR in an electrolysis cell. Moreover, given that the oxidation of HMF to FDCA is a six-electron transfer reaction, whereas the oxidation of glycerol to formic acid entails an eight-electron transfer, HMF should be a more ideal anode pairing for CO2RR.[37,230]

One of the first paired electrolysis systems combining simultaneous CO_2RR and HMF oxidation was reported by Bi *et al*.[271] PdOx/ZIF-8 and PdO were the cathode and the anode, respectively for an electrolyzer with an onset cell voltage of 1.06 V for efficient conversion of both CO_2 and HMF (1.77 V was need for conventional CO2RR-OER pairing). The FE reached 97% at 104 mA cm^{-2} for product yields of 20% for maleic acid and 64% for formic acid.[271] Nam's group synthesized 5 nm nickel oxide nanoparticles (NiO NPs) for the electrooxidation of HMF in a paired electrolysis system under neutral conditions (pH = 7.2) and at an onset potential of 1.52 V vs RHE (corresponding to a current density of 1 mA cm^{-2}), which is 0.15 V lower than that for OER (1.67 V vs RHE).[272] This system resulted in the reduction of CO_2 to formate using BiOx electrocatalysts combined with HMF oxidation to simultaneously produce FDCA. Electrolysis over 3 hours yielded a 36% HMF conversion and FE of up to 81% for formate production.[272]

Similar to section 4.1, to couple biomass electrolysis with CO_2 reduction (CO2RR), the number of electrons required to form a CO2RR molecule depends on the nature of the reaction product at the cathode, as explained by Professor Paul J. A. Kenis' team.[37] The lowest (simplest) case is where the CO2RR product is either formic acid or CO, representing 2 electrons per product molecule. When the CO2RR product is ethylene or ethanol, the number of electrons per product molecule is 12. Consequently, when the anodic process (biomass electrooxidation) requires a higher number of electrons, then during the full cell study, the challenge of electron transfer kinetics and mass transport becomes even more complex at high current densities (0.2 – 1 A cm^{-2}). We therefore argue that all claims should be accompanied by full-cell tests under a representative current density and using a fair electrode surface for normalization: metal foams versus flat/non-porous catalytic layer.[260] Finally, considering the different scenarios envisaged for the anode part (many options) and the cathode (HER,

CO2ORR, NRR) as well as the complexity of each pair of processes, we have deliberately not covered the capital/operating expenditure (CAPEX/OPEX) aspects, even though some studies are tackling them in the context of techno-economics studies,[37,202,273] and we will be devoting case studies thereto in the near future.

5. Conclusion and outlook

We have provided an overview and analysis of recent research on the electroconversion of biomass-based compounds, first in half-cell configurations and second in paired electrolysis systems. Indeed, replacing the slow oxygen evolution reaction (OER) within conventional water electrolysis cells with the oxidative upgrading of biomass feed-stocks is a sustainable, cost-effective and promising catalytic method for simultaneously producing high-value products and fuels. However, a number of key scientific and technical challenges still need to be addressed in the framework of future research. For example, when electroconversion of biomass (glucose, 5-hydroxymethylfurfural (HMF), cellulose, lignin, etc.) is combined with the main reduction reactions (HER, CO2RR, NRR, etc.) to electro-synthesize high-value chemicals (H_2, NH_3, ethylene, etc., at the cathode) as well as organic products (gluconate, 2,5-furandicarboxylic acid (FDCA), etc., at the anode), the nature of the biomass substrate and the nature of the reaction products targeted at the anode and cathode impact the number of electrons transferred per product molecule. The choice of electrode material and catalysts is of utmost importance, as unsuitable materials can result in slow reaction kinetics, reducing electron transfer during electrolysis under a representative current density (0.2 – 1 A cm^{-2}). Limitations in mass transfer can also arise from such cascades of proton-coupled electron transfer (PCET) processes, making it difficult to transport reactants (or products) to (or from) the electrode surface. Inefficient mass transfer can hamper the availability of reagents and fresh active sites on the electrode surface, affecting productivity and durability.

In order to optimize the electrocatalytic performance of the reactions occurring at both electrodes, it is necessary to understand the reaction pathways and identify the factors that control them. Among these factors, reactor design, membrane selection, and especially electrocatalyst fabrication have received considerable attention. The design of high-performance electrocatalysts is essential to steer the reaction in the appropriate direction (selectivity), improve reaction kinetics (activity) and increase system durability (stability). Although electrolysis of biomass and its derivates offers the potential to synthesize value-added chemicals beyond traditional water electrolysis, the reaction pathways of the biomass electrooxidation reactions can lead to many intermediates and by-products that are generated

along with the desired products. Therefore, improving selectivity is very important to avoid additional purification steps. A better understanding of the reaction mechanism might give a more accurate insight into the electrocatalysts development to achieve the desired reaction rate and product selectivity. For example, in situ or operando spectroscopic methods including S/TEM, Raman, FTIRS, XRD at the electrode/electrolyte interface play an irreplaceable role in the exploration of catalytic reaction mechanisms. In addition, theoretical calculations (e.g. DFT) can also help to further explore mechanisms and suggest promising active electrocatalysts for more efficient electrochemical conversion. Conceptually, all reactions can be paired in an electrolytic split cell, offering a wide range of possible combinations. However, it is worth assessing the feasibility of each combination in terms of cost (energy consumption, reactor configuration, catalysts and membranes) and the compatibility of the two reaction products (separation and purification).

For biomass-based paired electrosynthesis systems, basic fundamental research is still at the stage of small-scale experiments with miniaturized equipment, low current density and substrate addition at the millimolar level. In fact, most of the cited reports are performed at low current densities (< 0.1 A cm^{-2}, which allows to maximize the faradaic efficiency to the desired products and to avoid side reactions such as OER, complete oxidation of organics, and corrosion of the support (mostly carbon-based electrodes). However, to consider a scale-up application and to meet the requirements of industrial production, e.g. if sustainable H_2 production is targeted, high current densities (>0.2 A cm^{-2} to expect >0.1 L(H_2) h^{-1} cm^{-2}), high electrode surfaces and extensive reactors are necessary, which inevitably leads to higher operating costs and possible changes in reaction selectivity. To increase the final current density delivered, overcoming mass transport limitations by designing advanced continuous flow reactors and high performance electrocatalysts is the key to scalability. Although there is still room for further work to improve the processing for commercial-scale end-use applications, current research figures suggest that electrocatalytic upgrading of cellulosic biomass is a thoroughly prospective strategy for producing valuable energy carriers and/or chemical synthesis intermediates, among others.

To the open question of how do current electricity prices impact the overall feasibility and scalability of the biomass-fuelled paired electrosynthesis of valuable chemicals and fuels technologies, considering the energy-intensive nature of the electrochemical reactions involved, we suggest that the electrolyzers could be optimally deployed close to renewable energy sources such as solar, wind and hydro. Hence, during periods of peak production, excess electricity could be recovered/stored by powering the electrolyzer to produce, for example, H_2 or NH_3

fuels. This would enable us to capitalize on periods of peak electricity production (which are not fully utilized); for example, storage in the form of "fuel (such as H_2, NH_3)" during the summer for use during the winter, which would not be possible with batteries over a long period.

Acknowledgements

This work is supported by French National Research Agency through the project MASTERS (ANR-22-CE43-0004), Chimie Balard Cirimat Carnot institute through the ANR program N°16 CARN 0008-01 (project REMEC, 19S08R06-FPV-HOLADE), LabEx CheMISyst (ANR-10-LABX-0501) and Montpellier University of Excellence I-SITE (project NANOGATE).

Conflict of Interest

The authors declare no conflict of interest.

Received: ((will be filled in by the editorial staff))
Revised: ((will be filled in by the editorial staff))
Published online: ((will be filled in by the editorial staff))

References

[1] H.-O. Pörtner, D. Roberts, M. Tignor, E. Poloczanska, K. Mintenbeck, A. Alegría, M. Craig, S. Langsdorf, S. Löschke, V. Möller, A. Okem, B. Rama, D. Belling, W. Dieck, S. Götze, T. Kersher, P. Mangele, B. Maus, A. Mühle, N. Weyer, *Climate Change 2022: Impacts, Adaptation and Vulnerability Working Group II Contribution to the Sixth Assessment Report of the Intergovernmental Panel on Climate Change*, **2022**.
[2] F. Dawood, M. Anda, G. M. Shafiullah, *Int. J. Hydrogen Energy* **2020**, *45*, 3847.
[3] B. G. Pollet, S. S. Kocha, I. Staffell, *Curr. Opin. Electrochim* **2019**, *16*, 90.
[4] M. Chatenet, B. G. Pollet, D. R. Dekel, F. Dionigi, J. Deseure, P. Millet, R. D. Braatz, M. Z. Bazant, M. Eikerling, I. Staffell, *Chem. Soc. Rev.* **2022**, *51*, 4583.
[5] R. L. Germscheidt, D. E. B. Moreira, R. G. Yoshimura, N. P. Gasbarro, E. Datti, P. L. dos Santos, J. A. Bonacin, *Adv. Energy Sustainability Res.* **2021**, *2*, 2100093.
[6] N. Mamaca, E. Mayousse, S. Arrii-Clacens, T. W. Napporn, K. Servat, N. Guillet, K. B. Kokoh, *Appl. Catal. B: Env.* **2012**, *111-112*, 376.
[7] P. Millet, N. Mbemba, S. A. Grigoriev, V. N. Fateev, A. Aukauloo, C. Etiévant, *Int. J. Hydrogen Energy* **2011**, *36*, 4134.
[8] M. T. Dinh Nguyen, A. Ranjbari, L. Catala, F. Brisset, P. Millet, A. Aukauloo, *Coord. Chem. Rev.* **2012**, *256*, 2435.
[9] G. Jerkiewicz, *ACS Catal.* **2020**, *10*, 8409.
[10] B. Ahmed, M. J. Hossain, A. Al Parvez, A. Talukder, M. Al-Amin, M. A. Al Mahmud, T. Islam, *Adv. Energy Sustainability Res.* **First published: 15 December 2023**, 2300231.

[11] R. Boukil, N. Tuleushova, D. Cot, B. Rebiere, V. Bonniol, J. Cambedouzou, S. Tingry, D. Cornu, Y. Holade, *J. Mater. Chem. A* **2020**, *8*, 8848.
[12] Y. Holade, N. Tuleushova, S. Tingry, K. Servat, T. W. Napporn, H. Guesmi, D. Cornu, K. B. Kokoh, *Catal. Sci. Technol.* **2020**, *10*, 3071.
[13] Y. Kwon, S. C. S. Lai, P. Rodriguez, M. T. M. Koper, *J. Am. Chem. Soc.* **2011**, *133*, 6914.
[14] M. T. M. Koper, *Chem. Sci.* **2013**, *4*, 2710.
[15] S. C. S. Lai, S. E. F. Kleijn, F. T. Z. Öztürk, V. C. van Rees Vellinga, J. Koning, P. Rodriguez, M. T. M. Koper, *Catal. Today* **2010**, *154*, 92.
[16] I. Bodachivskyi, C. J. Page, U. Kuzhiumparambil, S. F. R. Hinkley, I. M. Sims, D. B. G. Williams, *ACS Sustainable Chem. Eng.* **2020**, *8*, 10142.
[17] S. Ramachandran, P. Fontanille, A. Pandey, C. Larroche, *Food Technol. Biotechnol.* **2006**, *44*, 185.
[18] P. Qi, S. Chen, J. Chen, J. Zheng, X. Zheng, Y. Yuan, *ACS Catal.* **2015**, *5*, 2659.
[19] H. Zhang, Y. Xu, Y. Li, Z. Lu, S. Cao, M. Fan, L. Huang, L. Chen, *Polymers* **2017**, *9*, 526.
[20] J. Zhou, L. Zhang, *Polym. J.* **2000**, *32*, 866.
[21] J. Miao, X. Teng, R. Zhang, P. Guo, Y. Chen, X. Zhou, H. Wang, X. Sun, L. Zhang, *Appl. Catal. B: Env.* **2020**, *263*, 118109.
[22] Y. Sugano, N. Kumar, M. Peurla, J. Roine, A. Aho, J. Bobacka, J.-P. Mikkola, *ChemCatChem* **2016**, *8*, 2401.
[23] T. Hibino, K. Kobayashi, M. Ito, M. Nagao, M. Fukui, S. Teranishi, *Appl. Catal. B: Env.* **2018**, *231*, 191.
[24] T. Hibino, K. Kobayashi, P. Lv, M. Nagao, S. Teranishi, *Bull. Chem. Soc. Jpn.* **2017**, *90*, 1017.
[25] Y. Kwon, S. E. F. Kleijn, K. J. P. Schouten, M. T. M. Koper, *ChemSusChem* **2012**, *5*, 1935.
[26] P. Parpot, V. P. Muiuane, V. Defontaine, A. P. Bettencourt, *Electrochim. Acta* **2010**, *55*, 3157.
[27] K. Park, P. N. Pintauro, M. M. Baizer, K. Nobe, *J. Electrochem. Soc.* **1985**, *132*, 1850.
[28] N. Sbei, T. Hardwick, N. Ahmed, *ACS Sustainable Chem. Eng.* **2021**, *9*, 6148.
[29] T. Fuchigami, M. Atobe, S. Inagi, *Fundamentals and Applications of Organic Electrochemistry: Synthesis, Materials, Devices*, John Wiley & Sons Ltd, Chichester, UK, **2014**.
[30] C. Kingston, M. D. Palkowitz, Y. Takahira, J. C. Vantourout, B. K. Peters, Y. Kawamata, P. S. Baran, *Acc. Chem. Res.* **2020**, *53*, 72.
[31] H. Sheng, A. N. Janes, R. D. Ross, H. Hofstetter, K. Lee, J. R. Schmidt, S. Jin, *Nat. Catal.* **2022**, *5*, 716.
[32] X. Dong, J. L. Roeckl, S. R. Waldvogel, B. Morandi, *Science* **2021**, *371*, 507.
[33] L. Wei, N. Tsutomu, *Chemistry Letters* **1997**, *26*, 1271.
[34] M. S. E. Houache, R. Safari, U. O. Nwabara, T. Rafaïdeen, G. A. Botton, P. J. A. Kenis, S. Baranton, C. Coutanceau, E. A. Baranova, *ACS Appl. Energy Mater.* **2020**, *3*, 8725.
[35] L. Tao, T. S. Choksi, W. Liu, J. Pérez-Ramírez, *ChemSusChem* **2020**, *13*, 6066.
[36] A. Bardow, M. Wessling, *Nat. Energy* **2019**, *4*, 440.
[37] S. Verma, S. Lu, P. J. A. Kenis, *Nat. Energy* **2019**, *4*, 466.
[38] P. D. Luna, C. Hahn, D. Higgins, S. A. Jaffer, T. F. Jaramillo, E. H. Sargent, *Science* **2019**, *364*, eaav3506.
[39] W.-J. Liu, Z. Xu, D. Zhao, X.-Q. Pan, H.-C. Li, X. Hu, Z.-Y. Fan, W.-K. Wang, G.-H. Zhao, S. Jin, G. W. Huber, H.-Q. Yu, *Nat. Commun.* **2020**, *11*, 265.

[40] Y. Kwon, K. J. P. Schouten, J. C. van der Waal, E. de Jong, M. T. M. Koper, *ACS Catal.* **2016**, *6*, 6704.
[41] N. Jiang, B. You, R. Boonstra, I. M. Terrero Rodriguez, Y. Sun, *ACS Energy Lett.* **2016**, *1*, 386.
[42] F. W. S. Lucas, R. G. Grim, S. A. Tacey, C. A. Downes, J. Hasse, A. M. Roman, C. A. Farberow, J. A. Schaidle, A. Holewinski, *ACS Energy Lett.* **2021**, *6*, 1205.
[43] M. Yang, Z. Yuan, R. Peng, S. Wang, Y. Zou, *Energy Environ. Mater.* **2022**, *5*, 1117.
[44] D. J. Chadderdon, L. Xin, J. Qi, Y. Qiu, P. Krishna, K. L. More, W. Li, *Green Chem.* **2014**, *16*, 3778.
[45] A. A. Rosatella, S. P. Simeonov, R. F. M. Frade, C. A. M. Afonso, *Green Chem.* **2011**, *13*, 754.
[46] T. Wang, L. Tao, X. Zhu, C. Chen, W. Chen, S. Du, Y. Zhou, B. Zhou, D. Wang, C. Xie, P. Long, W. Li, Y. Wang, R. Chen, Y. Zou, X.-Z. Fu, Y. Li, X. Duan, S. Wang, *Nat. Catal.* **2022**, *5*, 66.
[47] A. Caravaca, A. de Lucas-Consuegra, A. B. Calcerrada, J. Lobato, J. L. Valverde, F. Dorado, *Appl. Catal. B: Env.* **2013**, *134-135*, 302.
[48] T. Hibino, K. Kobayashi, M. Nagao, S. Teranishi, *ChemElectroChem* **2017**, *4*, 3032.
[49] S. Li, D. Liu, G. Wang, P. Ma, X. Wang, J. Wang, R. Ma, *Nano-Micro Lett.* **2023**, *15*, 189.
[50] J. Na, B. Seo, J. Kim, C. W. Lee, H. Lee, Y. J. Hwang, B. K. Min, D. K. Lee, H.-S. Oh, U. Lee, *Nat. Commun.* **2019**, *10*, 5193.
[51] E. Pérez-Gallent, S. Turk, R. Latsuzbaia, R. Bhardwaj, A. Anastasopol, F. Sastre-Calabuig, A. C. Garcia, E. Giling, E. Goetheer, *Ind. Eng. Chem. Res.* **2019**, *58*, 6195.
[52] J. Joo, T. Uchida, A. Cuesta, M. T. M. Koper, M. Osawa, *J. Am. Chem. Soc.* **2013**, *135*, 9991.
[53] B. N. Zope, D. D. Hibbitts, M. Neurock, R. J. Davis, *Science* **2010**, *330*, 74.
[54] W. C. Ketchie, M. Murayama, R. J. Davis, *Top. Catal.* **2007**, *44*, 307.
[55] A. J. Bard, L. R. Faulkner, H. S. White, *Electrochemical Methods: Fundamentals and Applications*, 3rd ed., John Wiley & Sons, Inc., USA, **2022**.
[56] A. J. Bard, L. R. Faulkner, *Electrochemical Methods: Fundamentals and Applications*, 1st ed., John Wiley & Sons, Inc., USA, **1980**.
[57] R. Francke, L. Gonzalez, R. D. Little, K. D. Moeller, in *Surface and Interface Science* (Ed.: K. Wandelt), Wiley‐VCH Verlag GmbH & Co. KGaA, Weinheim,Germany, **2020**, pp. 827.
[58] H. Liu, W. Li, *Curr. Opin. Electrochim* **2021**, *30*, 100795.
[59] S. Liang, N. Altaf, L. Huang, Y. Gao, Q. Wang, *J. CO2 Util.* **2020**, *35*, 90.
[60] K. P. Kuhl, E. R. Cave, D. N. Abram, T. F. Jaramillo, *Energy Environ. Sci.* **2012**, *5*, 7050.
[61] M. Rafiee, D. J. Abrams, L. Cardinale, Z. Goss, A. Romero-Arenas, S. S. Stahl, *Chem. Soc. Rev.* **2024**, https://doi.org/10.1039/D2CS00706A.
[62] R. G. Grim, Z. Huang, M. T. Guarnieri, J. R. Ferrell, L. Tao, J. A. Schaidle, *Energy Environ. Sci.* **2020**, *13*, 472.
[63] S. Anwar, F. Khan, Y. Zhang, A. Djire, *Int. J. Hydrogen Energy* **2021**, *46*, 32284.
[64] V. R. Stamenkovic, D. Strmcnik, P. P. Lopes, N. M. Markovic, *Nat. Mater.* **2017**, *16*, 57.
[65] J. K. Nørskov, T. Bligaard, A. Logadottir, J. R. Kitchin, J. G. Chen, S. Pandelov, U. Stimming, *J. Electrochem. Soc.* **2005**, *152*, J23.
[66] J. Greeley, J. K. Nørskov, L. A. Kibler, A. M. El-Aziz, D. M. Kolb, *ChemPhysChem* **2006**, *7*, 1032.

[67] Z. W. Seh, J. Kibsgaard, C. F. Dickens, I. Chorkendorff, J. K. Nørskov, T. F. Jaramillo, *Science* **2017**, *355*, eaad4998.
[68] D. W. Lima, F. Fiegenbaum, F. Trombetta, M. O. de Souza, E. M. A. Martini, *Int. J. Hydrogen Energy* **2017**, *42*, 5676.
[69] H. Liao, C. Wei, J. Wang, A. Fisher, T. Sritharan, Z. Feng, Z. J. Xu, *Adv. Energy Mater.* **2017**, *7*, 1701129.
[70] S. Xue, B. Garlyyev, S. Watzele, Y. Liang, J. Fichtner, M. D. Pohl, A. S. Bandarenka, *ChemElectroChem* **2018**, *5*, 2326.
[71] Y. Cheng, S. Lu, F. Liao, L. Liu, Y. Li, M. Shao, *Adv. Funct. Mater.* **2017**, *27*, 1700359.
[72] S. Zhou, H. Jang, Q. Qin, L. Hou, M. G. Kim, S. Liu, X. Liu, J. Cho, *Angew. Chem. Int. Ed.* **2022**, *61*, e202212196.
[73] J. Zheng, W. Sheng, Z. Zhuang, B. Xu, Y. Yan, *Sci. Adv.* **2016**, *2*, Article number: e1501602.
[74] Y. Holade, Z. H. Kavousi, M. Ghorbanloo, N. Masquelez, S. Tingry, D. Cornu, *Chem. Commun.* **2023**, *59*, 47.
[75] J.-F. Boue, C. Espinet, S. Amigues, D. Mesguich, D. Cornu, Y. Holade, J. Cambedouzou, C. Laurent, *Chem. Commun.* **2023**, *59*, 13719.
[76] J. Greeley, T. F. Jaramillo, J. Bonde, I. Chorkendorff, J. K. Norskov, *Nat. Mater.* **2006**, *5*, 909.
[77] J. Kibsgaard, Z. Chen, B. N. Reinecke, T. F. Jaramillo, *Nat. Mater.* **2012**, *11*, 963.
[78] X. Zou, Y. Zhang, *Chem. Soc. Rev.* **2015**, *44*, 5148.
[79] Y. Shi, B. Zhang, *Chem. Soc. Rev.* **2016**, *45*, 1529.
[80] S. Dresp, F. Dionigi, M. Klingenhof, P. Strasser, *ACS Energy Lett.* **2019**, *4*, 933.
[81] H. Xie, Z. Zhao, T. Liu, Y. Wu, C. Lan, W. Jiang, L. Zhu, Y. Wang, D. Yang, Z. Shao, *Nature* **2022**, 1.
[82] H. Minamihara, K. Kusada, D. Wu, T. Yamamoto, T. Toriyama, S. Matsumura, L. S. R. Kumara, K. Ohara, O. Sakata, S. Kawaguchi, *J. Am. Chem. Soc.* **2022**, *144*, 11525.
[83] Y. J. Qiao, M. Peng, J. Lan, K. Jiang, D. C. Chen, Y. W. Tan, *J. Mater. Chem. A* **2023**, *11*, 495.
[84] H. Shi, X. Y. Sun, S. P. Zeng, Y. Liu, G. F. Han, T. H. Wang, Z. Wen, Q. R. Fang, X. Y. Lang, Q. Jiang, *Small Struct.* **2023**, 8.
[85] Z. X. Cai, H. Goou, Y. Ito, T. Tokunaga, M. Miyauchi, H. Abe, T. Fujita, *Chem. Sci.* **2021**, *12*, 11306.
[86] Z. Wang, H. Wang, S. Ji, X. Wang, B. G. Pollet, R. Wang, *J. Power Sources* **2020**, *446*, 227348.
[87] Y. Wu, C. Sun, H. Wang, S. Ji, B. G. Pollet, J. Lu, X. Tian, H. Liang, X. Wang, R. Wang, *J. Alloys Compd.* **2022**, *903*, 163855.
[88] J. Xie, S. Li, X. Zhang, J. Zhang, R. Wang, H. Zhang, B. Pan, Y. Xie, *Chem. Sci.* **2014**, *5*, 4615.
[89] J. Shi, Z. Pu, Q. Liu, A. M. Asiri, J. Hu, X. Sun, *Electrochim. Acta* **2015**, *154*, 345.
[90] W. Kreuter, H. Hofmann, *Int. J. Hydrogen Energy* **1998**, *23*, 661.
[91] K. Zeng, D. Zhang, *Prog. Energy Combust. Sci.* **2010**, *36*, 307.
[92] J. K. Nørskov, T. Bligaard, A. Logadottir, J. R. Kitchin, J. G. Chen, S. Pandelov, U. Stimming, *J. Electrochem. Soc.* **2005**, *152*, J23.
[93] R. Li, K. Xiang, Z. Peng, Y. Zou, S. Wang, *Adv. Energy Mater.* **2021**, *11*, 2102292.
[94] K. Junge Puring, D. Siegmund, J. Timm, F. Möllenbruck, S. Schemme, R. Marschall, U.-P. Apfel, *Advanced Sustainable Systems* **2021**, *5*, 2000088.
[95] W. Zhong, W. Huang, S. Ruan, Q. Zhang, Y. Wang, S. Xie, *Chem. Eur. J.* **2023**, *29*, e202203228.

[96] J. Liu, X. Zhang, R. Yang, Y. Yang, X. Wang, *Adv. Energy Sustainability Res.* **2023**, *4*, 2200192.
[97] G. Wang, J. Chen, Y. Ding, P. Cai, L. Yi, Y. Li, C. Tu, Y. Hou, Z. Wen, L. Dai, *Chem. Soc. Rev.* **2021**, *50*, 4993.
[98] C. Costentin, M. Robert, J.-M. Savéant, *Chem. Soc. Rev.* **2013**, *42*, 2423.
[99] M. Balamurugan, L. Merakeb, K. T. Nam, M. Robert, in *Chemical Valorisation of Carbon Dioxide* (Eds.: G. Stefanidis, A. Stankiewicz), The Royal Society of Chemistry, **2022**, p. 0.
[100] S. Nitopi, E. Bertheussen, S. B. Scott, X. Liu, A. K. Engstfeld, S. Horch, B. Seger, I. E. L. Stephens, K. Chan, C. Hahn, J. K. Nørskov, T. F. Jaramillo, I. Chorkendorff, *Chem. Rev.* **2019**, *119*, 7610.
[101] J. He, K. E. Dettelbach, D. A. Salvatore, T. Li, C. P. Berlinguette, *Angew. Chem. Int. Ed.* **2017**, *56*, 6068.
[102] A. C. Garcia, C. Sánchez-Martínez, I. Bakker, E. Goetheer, *ACS Sustainable Chem. Eng.* **2020**, *8*, 10454.
[103] A. J. Medford, A. Vojvodic, J. S. Hummelshøj, J. Voss, F. Abild-Pedersen, F. Studt, T. Bligaard, A. Nilsson, J. K. Nørskov, *J. Catal.* **2015**, *328*, 36.
[104] S. Xie, W. Ma, X. Wu, H. Zhang, Q. Zhang, Y. Wang, Y. Wang, *Energy Environ. Sci.* **2021**, *14*, 37.
[105] V. Kyriakou, I. Garagounis, A. Vourros, E. Vasileiou, M. Stoukides, *Joule* **2020**, *4*, 142.
[106] A. J. Martín, T. Shinagawa, J. Pérez-Ramírez, *Chem* **2019**, *5*, 263.
[107] A. Valera-Medina, F. Amer-Hatem, A. K. Azad, I. C. Dedoussi, M. de Joannon, R. X. Fernandes, P. Glarborg, H. Hashemi, X. He, S. Mashruk, J. McGowan, C. Mounaim-Rouselle, A. Ortiz-Prado, A. Ortiz-Valera, I. Rossetti, B. Shu, M. Yehia, H. Xiao, M. Costa, *Energy Fuels* **2021**, *35*, 6964.
[108] G. Qing, R. Ghazfar, S. T. Jackowski, F. Habibzadeh, M. M. Ashtiani, C.-P. Chen, M. R. Smith, T. W. Hamann, *Chem. Rev.* **2020**, *120*, 5437.
[109] M. Capdevila-Cortada, *Nat. Catal.* **2019**, *2*, 1055.
[110] J. Nørskov, J. Chen, R. Miranda, T. Fitzsimmons, R. Stack, ; US DOE Office of Science, **2016**.
[111] J. G. Chen, R. M. Crooks, L. C. Seefeldt, K. L. Bren, R. M. Bullock, M. Y. Darensbourg, P. L. Holland, B. Hoffman, M. J. Janik, A. K. Jones, M. G. Kanatzidis, P. King, K. M. Lancaster, S. V. Lymar, P. Pfromm, W. F. Schneider, R. R. Schrock, *Science* **2018**, *360*, eaar6611.
[112] N. Gruber, J. N. Galloway, *Nature* **2008**, *451*, 293.
[113] M. Wang, M. A. Khan, I. Mohsin, J. Wicks, A. H. Ip, K. Z. Sumon, C.-T. Dinh, E. H. Sargent, I. D. Gates, M. G. Kibria, *Energy Environ. Sci.* **2021**, *14*, 2535.
[114] J. W. Erisman, M. A. Sutton, J. Galloway, Z. Klimont, W. Winiwarter, *Nature Geoscience* **2008**, *1*, 636.
[115] Y. Li, H. Wang, C. Priest, S. Li, P. Xu, G. Wu, *Adv. Mater.* **2021**, *33*, 2000381.
[116] R. F. Service, *Science* **2014**, *345*, 610.
[117] B. H. R. Suryanto, H.-L. Du, D. Wang, J. Chen, A. N. Simonov, D. R. MacFarlane, *Nat. Catal.* **2019**, *2*, 290.
[118] R. Service, *Science* **2018**, aau7489.
[119] J. Humphreys, R. Lan, S. Tao, *Adv. Energy Sustainability Res.* **2021**, *2*, 2000043.
[120] X. Li, T. Li, Y. Ma, Q. Wei, W. Qiu, H. Guo, X. Shi, P. Zhang, A. M. Asiri, L. Chen, B. Tang, X. Sun, *Adv. Energy Mater.* **2018**, *8*, 1801357.
[121] D. Gupta, A. Kafle, T. C. Nagaiah, *Small* **2023**, *19*, 2208272.
[122] R. Li, T. Li, X. Liu, C. Xie, Q. Zhen, S. Bashir, J. L. Liu, *Energy Science & Engineering* **2023**, *11*, 2293.

[123] H. Jin, S. S. Kim, S. Venkateshalu, J. Lee, K. Lee, K. Jin, *Adv. Sci.* **2023**, *10*, 2300951.
[124] R. D. Milton, S. D. Minteer, *Acc. Chem. Res.* **2019**, *52*, 3351.
[125] C. Cadoux, D. Ratcliff, N. Maslać, W. Gu, I. Tsakoumagkos, S. Hoogendoorn, T. Wagner, R. D. Milton, *JACS Au* **2023**, *3*, 1521.
[126] J. S. Anderson, J. Rittle, J. C. Peters, *Nature* **2013**, *501*, 84.
[127] L. C. Seefeldt, B. M. Hoffman, D. R. Dean, *Annu. Rev. Biochem.* **2009**, *78*, 701.
[128] B. M. Hoffman, D. R. Dean, L. C. Seefeldt, *Acc. Chem. Res.* **2009**, *42*, 609.
[129] O. Einsle, F. A. Tezcan, S. L. A. Andrade, B. Schmid, M. Yoshida, J. B. Howard, D. C. Rees, *Science* **2002**, *297*, 1696.
[130] V. K. Shah, W. J. Brill, *Proc. Natl. Acad. Sci.* **1977**, *74*, 3249.
[131] S. D. Minteer, P. Christopher, S. Linic, *ACS Energy Lett.* **2019**, *4*, 163.
[132] S. L. Foster, S. I. P. Bakovic, R. D. Duda, S. Maheshwari, R. D. Milton, S. D. Minteer, M. J. Janik, J. N. Renner, L. F. Greenlee, *Nat. Catal.* **2018**, *1*, 490.
[133] E. Skúlason, T. Bligaard, S. Gudmundsdóttir, F. Studt, J. Rossmeisl, F. Abild-Pedersen, T. Vegge, H. Jónsson, J. K. Nørskov, *Phys. Chem. Chem. Phys.* **2012**, *14*, 1235.
[134] A. R. Singh, B. A. Rohr, J. A. Schwalbe, M. Cargnello, K. Chan, T. F. Jaramillo, I. Chorkendorff, J. K. Nørskov, *ACS Catal.* **2017**, *7*, 706.
[135] H.-P. Jia, E. A. Quadrelli, *Chem. Soc. Rev.* **2014**, *43*, 547.
[136] M. Wei, S. Li, X. Wang, G. Zuo, H. Wang, X. Meng, J. Wang, *Adv. Energy Sustainability Res.* **2023**, *DOI: https://doi.org/10.1002/aesr.202300173*, 2300173.
[137] H. Wang, J. Huang, J. Cai, Y. Wei, A. Cao, B. Liu, S. Lu, *Small Methods* **2023**, *7*, 2300169.
[138] H. Xu, J. Wu, W. Luo, Q. Li, W. Zhang, J. Yang, *Small* **2020**, *16*, 2001775.
[139] L. Sun, B. Liu, *Adv. Mater.* **2023**, *35*, 2207305.
[140] S. Liu, X. Zheng, T. Jiang, W. Chen, in *Encyclopedia of Nanomaterials (First Edition)* (Eds.: Y. Yin, Y. Lu, Y. Xia), Elsevier, Oxford, **2023**, pp. 590.
[141] R. Paul, L. Zhu, H. Chen, J. Qu, L. Dai, *Adv. Mater.* **2019**, *31*, 1806403.
[142] S. K. Ghosh, H. Rahaman, in *Noble Metal-Metal Oxide Hybrid Nanoparticles* (Eds.: S. Mohapatra, T. A. Nguyen, P. Nguyen-Tri), Woodhead Publishing, **2019**, pp. 313.
[143] G.-R. Zhang, C. Yong, L.-L. Shen, H. Yu, K. Brunnengräber, T. Imhof, D. Mei, B. J. M. Etzold, *ACS Appl. Mater. Interfaces.* **2023**, *15*, 18781.
[144] A. C. Garcia, T. Touzalin, C. Nieuwland, N. Perini, M. T. M. Koper, *Angew. Chem. Int. Ed.* **2019**, *58*, 12999.
[145] C. Lin, P. Zhang, S. Wang, Q. Zhou, B. Na, H. Li, J. Tian, Y. Zhang, C. Deng, L. Meng, J. Wu, C. Liu, J. Hu, L. Zhang, *J. Alloys Compd.* **2020**, *823*, 153784.
[146] C. Yu, J. Lu, L. Luo, F. Xu, P. K. Shen, P. Tsiakaras, S. Yin, *Electrochim. Acta* **2019**, *301*, 449.
[147] Z.-F. Huang, J. Song, Y. Du, S. Xi, S. Dou, J. M. V. Nsanzimana, C. Wang, Z. J. Xu, X. Wang, *Nat. Energy* **2019**, *4*, 329.
[148] L. Trotochaud, S. L. Young, J. K. Ranney, S. W. Boettcher, *J. Am. Chem. Soc.* **2014**, *136*, 6744.
[149] M. Görlin, P. Chernev, P. Paciok, C.-W. Tai, J. Ferreira de Araújo, T. Reier, M. Heggen, R. Dunin-Borkowski, P. Strasser, H. Dau, *Chem. Commun.* **2019**.
[150] D. Dekel, in *Encyclopedia of Applied Electrochemistry* (Eds.: G. Kreysa, K.-i. Ota, R. F. Savinell), Springer New York, New York, NY, **2014**, pp. 33.
[151] J. R. Varcoe, P. Atanassov, D. R. Dekel, A. M. Herring, M. A. Hickner, P. A. Kohl, A. R. Kucernak, W. E. Mustain, K. Nijmeijer, K. Scott, T. Xu, L. Zhuang, *Energy Environ. Sci.* **2014**, *7*, 3135.

[152] S. Dresp, T. N. Thanh, M. Klingenhof, S. Bruckner, P. Hauke, P. Strasser, *Energy Environ. Sci.* **2020**, *13*, 1725.
[153] R. Subbaraman, D. Tripkovic, K.-C. Chang, D. Strmcnik, A. P. Paulikas, P. Hirunsit, M. Chan, J. Greeley, V. Stamenkovic, N. M. Markovic, *Nat. Mater.* **2012**, *11*, 550.
[154] R. Vinodh, S. S. Kalanur, S. K. Natarajan, B. G. Pollet, *Polymers* **2023**, *15*, 2144.
[155] J. Müller, A. Zhegur, U. Krewer, J. R. Varcoe, D. R. Dekel, *ACS Mater. Lett.* **2020**, *2*, 168.
[156] N. Chen, C. Hu, H. H. Wang, J. H. Park, H. M. Kim, Y. M. Lee, *J. Membrane Sci.* **2021**, *638*, 119685.
[157] X. Wang, R. G. H. Lammertink, *J. Mater. Chem. A* **2022**, *10*, 8401.
[158] M. M. Hossain, L. Wu, X. Liang, Z. Yang, J. Hou, T. Xu, *J. Power Sources* **2018**, *390*, 234.
[159] S. Sung, J. E. Chae, K. Min, H.-J. Kim, S. Y. Nam, T.-H. Kim, *J. Mater. Chem. A* **2021**, *9*, 1062.
[160] Y. Kim, Y. Wang, A. France-Lanord, Y. Wang, Y.-C. M. Wu, S. Lin, Y. Li, J. C. Grossman, T. M. Swager, *J. Am. Chem. Soc.* **2019**, *141*, 18152.
[161] N. Chen, Q. Jiang, F. Song, X. Hu, *ACS Energy Lett.* **2023**, 4043.
[162] P. Mardle, B. Chen, S. Holdcroft, *ACS Energy Lett.* **2023**, 3330.
[163] Y. Zheng, A. Serban, H. Zhang, N. Chen, F. Song, X. Hu, *ACS Energy Lett.* **2023**, 5018.
[164] J. Li, C. Liu, J. Ge, W. Xing, J. Zhu, *Chem. Eur. J.* **2023**, *29*, e202203173.
[165] D. Henkensmeier, M. Najibah, C. Harms, J. Žitka, J. Hnát, K. Bouzek, *J. Electrochem. Energy Convers. Storage* **2020**, *18*.
[166] L. Wang, X. Peng, W. E. Mustain, J. R. Varcoe, *Energy Environ. Sci.* **2019**, *12*, 1575.
[167] C. Shang, Z. Wang, L. Wang, J. Wang, *Int. J. Hydrogen Energy* **2020**, *45*, 16738.
[168] A. Zhegur-Khais, F. Kubannek, U. Krewer, D. R. Dekel, *J. Membrane Sci.* **2020**, *612*, 118461.
[169] J. C. Douglin, R. K. Singh, S. Haj-Bsoul, S. Li, J. Biemolt, N. Yan, J. R. Varcoe, G. Rothenberg, D. R. Dekel, *Chem. Eng. J. Adv.* **2021**, *8*, 100153.
[170] A. G. Wright, J. Fan, B. Britton, T. Weissbach, H.-F. Lee, E. A. Kitching, T. J. Peckham, S. Holdcroft, *Energy Environ. Sci.* **2016**, *9*, 2130.
[171] N. Ziv, D. R. Dekel, *Electrochem. Commun.* **2018**, *88*, 109.
[172] N. Ziv, W. E. Mustain, D. R. Dekel, *ChemSusChem* **2018**, *11*, 1136.
[173] J. Huang, A. Malek, J. Zhang, M. H. Eikerling, *J. Phys. Chem. C* **2016**, *120*, 13587.
[174] Z. Liu, S. D. Sajjad, Y. Gao, H. Yang, J. J. Kaczur, R. I. Masel, *Int. J. Hydrogen Energy* **2017**, *42*, 29661.
[175] B. Motealleh, Z. Liu, R. I. Masel, J. P. Sculley, Z. Richard Ni, L. Meroueh, *Int. J. Hydrogen Energy* **2021**, *46*, 3379.
[176] Y. Chen, C. Liu, J. Xu, C. Xia, P. Wang, B. Y. Xia, Y. Yan, X. Wang, *Small Struct.* **2023**, *4*, 2200130.
[177] H. Cho, S. Moon Kim, Y. Sik Kang, J. Kim, S. Jang, M. Kim, H. Park, J. Won Bang, S. Seo, K.-Y. Suh, Y.-E. Sung, M. Choi, *Nat. Commun.* **2015**, *6*, Article number: 8484.
[178] L. A. M. Riascos, *J. Power Sources* **2008**, *184*, 204.
[179] Y. Sone, P. Ekdunge, D. Simonsson, *J. Electrochem. Soc.* **1996**, *143*, 1254.
[180] S. Sen, J. D. Martin, D. S. Argyropoulos, *ACS Sustainable Chem. Eng.* **2013**, *1*, 858.
[181] M. Jarvis, *Nature* **2003**, *426*, 611.
[182] A. H. Tayeb, E. Amini, S. Ghasemi, M. Tajvidi, *Molecules* **2018**, *23*, 2684.
[183] I. M. SAXENA, R. M. BROWN, JR, *Ann. Bot.* **2005**, *96*, 9.
[184] E. M. Debzi, H. Chanzy, J. Sugiyama, P. Tekely, G. Excoffier, *Macromolecules* **1991**, *24*, 6816.

[185] X. Qian, S.-Y. Ding, M. R. Nimlos, D. K. Johnson, M. E. Himmel, *Macromolecules* **2005**, *38*, 10580.
[186] S. Kobayashi, S.-i. Shoda, *Int. J. Biol. Macromol.* **1995**, *17*, 373.
[187] D. An, A. Ye, W. Deng, Q. Zhang, Y. Wang, *Chem. Eur. J.* **2012**, *18*, 2938.
[188] Y. Nishiyama, J. Sugiyama, H. Chanzy, P. Langan, *J. Am. Chem. Soc.* **2003**, *125*, 14300.
[189] H. Xiao, M. Wu, G. Zhao, *Catalysts* **2016**, *6*, 5.
[190] L. Yan, X. Qi, *ACS Sustainable Chem. Eng.* **2014**, *2*, 897.
[191] J. Zhou, L. Zhang, *Polym. J.* **2000**, *32*, 866.
[192] T. Heinze, O. A. El Seoud, A. Koschella, in *Cellulose Derivatives: Synthesis, Structure, and Properties*, Springer International Publishing, Cham, **2018**, pp. 173.
[193] S. Sen, B. P. Losey, E. E. Gordon, D. S. Argyropoulos, J. D. Martin, *J. Phys. Chem. B* **2016**, *120*, 1134.
[194] M. T. Clough, K. Geyer, P. A. Hunt, S. Son, U. Vagt, T. Welton, *Green Chem.* **2015**, *17*, 231.
[195] I. Bodachivskyi, U. Kuzhiumparambil, D. B. G. Williams, *ChemSusChem* **2018**, *11*, 642.
[196] M. T. Clough, K. Geyer, P. A. Hunt, J. Mertes, T. Welton, *Phys. Chem. Chem. Phys.* **2013**, *15*, 20480.
[197] R. S. Payal, S. Balasubramanian, *Phys. Chem. Chem. Phys.* **2014**, *16*, 17458.
[198] A. Brandt, J. Gräsvik, J. P. Hallett, T. Welton, *Green Chem.* **2013**, *15*, 550.
[199] R. P. Swatloski, S. K. Spear, J. D. Holbrey, R. D. Rogers, *J. Am. Chem. Soc.* **2002**, *124*, 4974.
[200] O. M. Gazit, A. Katz, *ChemSusChem* **2012**, *5*, 1542.
[201] A. Michud, M. Hummel, S. Haward, H. Sixta, *Carbohydrate Polymers* **2015**, *117*, 355.
[202] M. A. Khan, T. A. Al-Attas, N. G. Yasri, H. Zhao, S. Larter, J. Hu, M. G. Kibria, *Sustainable Energy Fuels* **2020**, *4*, 5568.
[203] G. Moggia, T. Kenis, N. Daems, T. Breugelmans, *ChemElectroChem* **2020**, *7*, 86.
[204] Y. Holade, A. B. Engel, K. Servat, T. W. Napporn, C. Morais, S. Tingry, D. Cornu, K. B. Kokoh, *J. Electrochem. Soc.* **2018**, *165*, H425.
[205] A. S. Ben, T. Isao, *Chemistry Letters* **2008**, *37*, 936.
[206] M. Pasta, R. Ruffo, E. Falletta, C. M. Mari, C. D. Pina, *Gold Bull.* **2010**, *43*, 57.
[207] L. Ostervold, S. I. Perez Bakovic, J. Hestekin, L. F. Greenlee, *RSC Adv.* **2021**, *11*, 31208.
[208] D. Li, Y. Huang, Z. Li, L. Zhong, C. Liu, X. Peng, *Chem. Eng. J.* **2022**, *430*, 132783.
[209] Y.-Q. Zhu, H. Zhou, J. Dong, S.-M. Xu, M. Xu, L. Zheng, Q. Xu, L. Ma, Z. Li, M. Shao, H. Duan, *Angew. Chem. Int. Ed.* **2023**, *62*, e202219048.
[210] S. Hebié, T. W. Napporn, C. Morais, K. B. Kokoh, *ChemPhysChem* **2016**, *17*, 1454.
[211] Y. Holade, K. Servat, T. W. Napporn, K. B. Kokoh, *Electrochim. Acta* **2015**, *162*, 205.
[212] C. Lemoine, Y. Holade, L. Dubois, T. W. Napporn, K. Servat, K. B. Kokoh, *J. Electroanal. Chem.* **2021**, *887*, Article number: 115162.
[213] Y. Holade, K. Servat, S. Tingry, T. W. Napporn, H. Remita, D. Cornu, K. B. Kokoh, *ChemPhysChem* **2017**, *18*, 2573.
[214] Y. Holade, S. Hebié, K. Maximova, M. Sentis, P. Delaporte, K. B. Kokoh, T. W. Napporn, A. V. Kabashin, *Catal. Sci. Technol.* **2020**, *10*, 7955.
[215] S. Hebié, K. B. Kokoh, K. Servat, T. Napporn, *Gold Bull.* **2013**, *46*, 311.
[216] T. Rafaïdeen, S. Baranton, C. Coutanceau, *Appl. Catal. B: Env.* **2019**, *243*, 641.
[217] Z. Wang, P. Liu, J. Han, C. Cheng, S. Ning, A. Hirata, T. Fujita, M. Chen, *Nat. Commun.* **2017**, *8*, 1066.

[218] N. Arjona, G. Trejo, J. Ledesma-García, L. G. Arriaga, M. Guerra-Balcázar, *RSC Adv.* **2016**, *6*, 15630.
[219] Y. Holade, H. Guesmi, J.-S. Filhol, Q. Wang, T. Pham, J. Rabah, E. Maisonhaute, V. Bonniol, K. Servat, S. Tingry, D. Cornu, K. B. Kokoh, T. W. Napporn, S. D. Minteer, *ACS Catal.* **2022**, *12*, 12563.
[220] L. Oliva, J. A. Fernandez-Lopez, X. Remesar, M. Alemany, *J. Endocrinol. Metab.* **2019**, *9*, 63.
[221] J. U. N. Okuda, T. Taguchi, A. Tomimura, *Chem. Pharm. Bull. (Tokyo)* **1987**, *35*, 4332.
[222] M. W. Hsiao, R. R. Adžić, E. B. Yeager, *J. Electrochem. Soc.* **1996**, *143*, 759.
[223] F. Largeaud, K. B. Kokoh, B. Beden, C. Lamy, *J. Electroanal. Chem.* **1995**, *397*, 261.
[224] A. Caglar, D. Düzenli, I. Onal, I. Tezsevin, O. Sahin, H. Kivrak, *Int. J. Hydrogen Energy* **2020**, *45*, 490.
[225] L. Wei, T. Sheng, J.-Y. Ye, B.-A. Lu, N. Tian, Z.-Y. Zhou, X.-S. Zhao, S.-G. Sun, *Langmuir* **2017**, *33*, 6991.
[226] T. Faverge, B. Gilles, A. Bonnefont, F. Maillard, C. Coutanceau, M. Chatenet, *ACS Catal.* **2023**, *13*, 2657.
[227] S. Cheng, H. Zhong, F. Jin, *Energy Science & Engineering* **2023**, *11*, 2944.
[228] A. J. J. E. Eerhart, A. P. C. Faaij, M. K. Patel, *Energy Environ. Sci.* **2012**, *5*, 6407.
[229] J. J. Bozell, G. R. Petersen, *Green Chem.* **2010**, *12*, 539.
[230] Y. Yang, T. Mu, *Green Chem.* **2021**, *23*, 4228.
[231] Y. Lu, T. Liu, C.-L. Dong, C. Yang, L. Zhou, Y.-C. Huang, Y. Li, B. Zhou, Y. Zou, S. Wang, *Adv. Mater.* **2022**, *34*, 2107185.
[232] D. H. Nam, B. J. Taitt, K. S. Choi, *ACS Catal.* **2018**, *8*, 1197.
[233] S. R. Kubota, K.-S. Choi, *ChemSusChem* **2018**, *11*, 2138.
[234] C. Wang, H.-J. Bongard, C. Weidenthaler, Y. Wu, F. Schüth, *Chem. Mater.* **2022**, *34*, 3123.
[235] L. Gao, S. Gan, J. Ma, Z. Sun, Z. Liu, L. Zhong, K. Zhou, F. Han, W. Wang, D. Han, L. Niu, *ChemElectroChem* **2020**, *7*, 4251.
[236] M. Park, M. Gu, B.-S. Kim, *ACS Nano* **2020**, *14*, 6812.
[237] K. Li, Y. J. Sun, *Chem.-Eur. J.* **2018**, *24*, 18258.
[238] L. F. Gao, Z. B. Liu, J. L. Ma, L. J. Zhong, Z. Q. Song, J. A. Xu, S. Y. Gan, D. X. Han, L. Niu, *Appl. Catal. B-Environ.* **2020**, *261*, 8.
[239] A. R. Poerwoprajitno, L. Gloag, J. Watt, S. Cychy, S. Cheong, P. V. Kumar, T. M. Benedetti, C. Deng, K. H. Wu, C. E. Marjo, D. L. Huber, M. Muhler, J. J. Gooding, W. Schuhmann, D. W. Wang, R. D. Tilley, *Angew. Chem.-Int. Edit.* **2020**, *59*, 15487.
[240] H. Wang, C. Li, J. An, Y. Zhuang, S. Tao, *J. Mater. Chem. A* **2021**, *9*, 18421.
[241] X. Lu, K.-H. Wu, B. Zhang, J. Chen, F. Li, B.-J. Su, P. Yan, J.-M. Chen, W. Qi, *Angew. Chem. Int. Ed.* **2021**, *60*, 14528.
[242] Z. Yang, B. Zhang, C. Yan, Z. Xue, T. Mu, *Appl. Catal. B: Env.* **2023**, *330*, 122590.
[243] Z. Yang, S. Wang, C. Wei, L. Chen, Z. Xue, T. Mu, *Energy Environ. Sci.* **2024**, *17*, 1603.
[244] M. Chávez Morejón, N. Kurig, Y. S. Tschauder, F. Harnisch, R. Palkovits, *ChemistrySelect* **2023**, *8*, e202301823.
[245] P. Parpot, K. Servat, A. P. Bettencourt, H. Huser, K. B. Kokoh, *Cellulose* **2010**, *17*, 815.
[246] Y. Sugano, M. d. Vestergaard, H. Yoshikawa, M. Saito, E. Tamiya, *Electroanalysis* **2010**, *22*, 1688.
[247] Y. Sugano, R.-M. Latonen, M. Akieh-Pirkanniemi, J. Bobacka, A. Ivaska, *ChemSusChem* **2014**, *7*, 2240.

[248] T. Hibino, K. Kobayashi, M. Ito, Q. Ma, M. Nagao, M. Fukui, S. Teranishi, *ACS Sustainable Chem. Eng.* **2018**, *6*, 9360.
[249] W. Liu, Y. Cui, X. Du, Z. Zhang, Z. Chao, Y. Deng, *Energy Environ. Sci.* **2016**, *9*, 467.
[250] H. Xiao, M. Wu, G. Zhao, *Catalysts* **2016**, *6*, Article number: 5.
[251] J. Zakzeski, P. C. A. Bruijnincx, A. L. Jongerius, B. M. Weckhuysen, *Chem. Rev.* **2010**, *110*, 3552.
[252] Y. Li, Z. Dang, P. Gao, *Nano Select* **2021**, *2*, 847.
[253] S. Stiefel, A. Schmitz, J. Peters, D. Di Marino, M. Wessling, *Green Chem.* **2016**, *18*, 4999.
[254] P. Cai, H. Fan, S. Cao, J. Qi, S. Zhang, G. Li, *Electrochim. Acta* **2018**, *264*, 128.
[255] Y.-m. Zhang, Y. Peng, X.-l. Yin, Z.-h. Liu, G. Li, *J. Chem. Technol. Biotechnol.* **2014**, *89*, 1954.
[256] M. Garedew, D. Young-Farhat, S. Bhatia, P. Hao, J. E. Jackson, C. M. Saffron, *Sustainable Energy Fuels* **2020**, *4*, 1340.
[257] S. Stiefel, J. Lölsberg, L. Kipshagen, R. Möller-Gulland, M. Wessling, *Electrochem. Commun.* **2015**, *61*, 49.
[258] B. Bawareth, D. Di Marino, T. A. Nijhuis, T. Jestel, M. Wessling, *ACS Sustainable Chem. Eng.* **2019**, *7*, 2091.
[259] M. Garedew, F. Lin, B. Song, T. M. DeWinter, J. E. Jackson, C. M. Saffron, C. H. Lam, P. T. Anastas, *ChemSusChem* **2020**, *13*, 4214.
[260] W. Zheng, M. Liu, L. Y. S. Lee, *ACS Energy Lett.* **2020**, *5*, 3260.
[261] N. Jiang, X. Liu, J. Dong, B. You, X. Liu, Y. Sun, *ChemNanoMat* **2017**, *3*, 491.
[262] S. R. Kubota, K.-S. Choi, *ACS Sustainable Chem. Eng.* **2018**, *6*, 9596.
[263] B. You, X. Liu, N. Jiang, Y. Sun, *J. Am. Chem. Soc.* **2016**, *138*, 13639.
[264] N. Zhang, Y. Zou, L. Tao, W. Chen, L. Zhou, Z. Liu, B. Zhou, G. Huang, H. Lin, S. Wang, *Angew. Chem. Int. Ed.* **2019**, *58*, 15895.
[265] Y. Song, Z. Li, K. Fan, Z. Ren, W. Xie, Y. Yang, M. Shao, M. Wei, *Appl. Catal. B: Env.* **2021**, *299*, 120669.
[266] Y. Song, W. Xie, Y. Song, H. Li, S. Li, S. Jiang, J. Y. Lee, M. Shao, *Appl. Catal. B: Env.* **2022**, *312*, 121400.
[267] H. Zhou, Y. Ren, B. Yao, Z. Li, M. Xu, L. Ma, X. Kong, L. Zheng, M. Shao, H. Duan, *Nat. Commun.* **2023**, *14*, 5621.
[268] G.-R. Xu, M. Batmunkh, S. Donne, H. Jin, J.-X. Jiang, Y. Chen, T. Ma, *J. Mater. Chem. A* **2019**, *7*, 25433.
[269] Q. Qin, T. Heil, J. Schmidt, M. Schmallegger, G. Gescheidt, M. Antonietti, M. Oschatz, *ACS Appl. Energy Mater.* **2019**, *2*, 8359.
[270] Y. Zheng, A. Vasileff, X. Zhou, Y. Jiao, M. Jaroniec, S.-Z. Qiao, *J. Am. Chem. Soc.* **2019**, *141*, 7646.
[271] J. Bi, Q. Zhu, W. Guo, P. Li, S. Jia, J. Liu, J. Ma, J. Zhang, Z. Liu, B. Han, *ACS Sustainable Chem. Eng.* **2022**, *10*, 8043.
[272] S. Choi, M. Balamurugan, K.-G. Lee, K. H. Cho, S. Park, H. Seo, K. T. Nam, *J. Phys. Chem. Lett.* **2020**, *11*, 2941.
[273] S. K. Nabil, M. A. Muzibur Raghuman, K. Kannimuthu, M. Rashid, H. S. Shiran, M. G. Kibria, M. A. Khan, *Nat. Catal.* **2024**.

Amira Ben Abderrahmane is a PhD student working on the development of electrocatalysts for the selective electroconversion of cellulosic biomass into synthons in a hydrogen co-production electrolyzer at the European Institute of Membranes of Montpellier (IEM, France). Her project aims to contribute to the development of new sustainable, low-carbon technologies to meet the challenges of the energy transition. As for her background, she obtained her Bachelor (2020) and Master's degree (2022) in Materials Chemistry at Sorbonne University (Paris).

Sophie Tingry obtained her PhD in Electrochemistry at the University of Grenoble (1996, France). She got a tenured position as CNRS researcher in 2000 at the European Membrane Institute of Montpellier (IEM), and she was promoted director of research in 2017. Her current research interests focus on the development of energy harvesting and (bio)sensor systems.

David Cornu obtained his PhD at the University of Lyon 1 (1998, France), where he was an assistant professor (1999-2008). Since 2008, he is full professor at the National School of Chemistry of Montpellier (ENSCM, University of Montpellier, France) and develops his research activities at the European Membrane Institute of Montpellier (IEM) with a focus on nanomaterials as membrane building blocks for biotechnology, health and energy applications. He was appointed director of the IEM Montpellier in 2021.

Yaovi Holade began his love of Electrochemistry at the University of Poitiers (France) where he received his Ph.D. in 2015 (supervision of Prof. Boniface K. Kokoh and Dr. Karine Servat). After a postdoctoral stint with Shelley D. Minteer at University of Utah (USA, 2015−2016) in bioelectrochemistry, he started his independent career as an Assistant Professor in 2016, and since 2023 he is Associate Professor at National Graduate School of Chemistry

of Montpellier (ENSCM) and European Institute of Membranes of Montpellier (IEM). His research interests include electrocatalysts development for electrolyzers and fuel cells, the galvanic replacement phenomena and the electro-valorization of biomass.

The table of contents entry

For the efficient utilization of renewable electrical energy in an electrolyzer, the anodic and cathodic reactions could play a crucial role in paired electrosynthesis systems. This review highlights the current research progress and major challenges in combining biomass electrooxidation with reduction reactions (HER, CO2RR, NRR), which can not only minimize energy consumption but also produce valuable chemicals and fuels.

*Amira Ben Abderrahmane, Sophie Tingry, David Cornu and Yaovi Holade**

Progress on Biomass Electro-Valorization for Paired Electrosynthesis of Valuable Chemicals and Fuels

ToC figure